Intravitreal application of AAV-BDNF or mutant AAV-CRMP2 protects retinal ganglion cells and stabilizes axons and myelin after partial optic nerve injury

Wissam Chiha[1,4], Carole Bartlett[1], Steven Petratos[5], Melinda Fitzgerald [3,4], Alan R. Harvey [2,3]

[1]*School of Biological Sciences, The University of Western Australia, WA 6009.*

[2]*School of Human Sciences, The University of Western Australia, WA 6009*

[3]*Perron Institute for Neurological and Translational Science, Nedlands, WA 6009.*

[4] *Curtin Health Innovation Research Institute, Curtin University, Belmont, WA 6102.*

[5]*Department of Neuroscience, Monash University, VIC 3004*

Abstract

Secondary degeneration following an initial injury to the central nervous system (CNS) results in increased tissue loss and is associated with increasing functional impairment. Unilateral partial dorsal transection of the adult rat optic nerve (ON) has proved to be a useful experimental model in which to study factors that contribute to secondary degenerative events. Using this injury model, we here quantified the protective effects of intravitreally administered bi-*cis*tronic adeno-associated viral (AAV2) vectors encoding either brain derived neurotrophic factor (BDNF) or a mutant, phospho-resistant, version of collapsin response mediator protein 2 (CRMP2T555A) on retinal ganglion cells (RGCs), their axons, and associated myelin. To test for potential synergistic interactions, some animals received combined injections of both vectors. Three months post-injury, all treatments maintained RGC numbers in central retina, but only AAV2-BDNF significantly protected ventrally located RGCs exclusively vulnerable to secondary degeneration. Behaviourally, treatments that involved AAV2-BDNF significantly restored the number of smooth-pursuit phases of optokinetic nystagmus. While all therapeutic regimens preserved axonal density and proportions of typical complexes, including heminodes and single nodes, BDNF treatments were generally more effective in maintaining the length of the node of Ranvier in myelin surrounding ventral ON axons after injury. Both AAV2-BDNF and AAV2-CRMP2T555A prevented injury-induced changes in G-ratio and overall myelin thickness, but only AAV2-BDNF administration protected against large-scale myelin decompaction in ventral ON. In summary, in a model of secondary CNS degeneration, both BDNF and CRMP2T555A vectors were neuroprotective, however different efficacies were observed for these overexpressed proteins in the retina and ON, suggesting disparate cellular and molecular targets driving responses for neural repair. The potential use of these vectors to treat other CNS injuries and pathologies is discussed.

Key words

Secondary degeneration, collapsin response mediator protein 2, brain derived neurotrophic factor, retinal ganglion cells, adeno-associated viral vector, gene therapy

Introduction

The injured central nervous system (CNS) of adult mammals has only a limited capacity to regenerate. Trauma to the brain and spinal cord creates a neural environment adversely affected by intrinsic and extrinsic factors that together induce degeneration and restrict regrowth. After an injury, secondary pathological events further compromise adjacent initially intact tissue, triggering homeostatic system disruptions and culminating in widespread cell death, axonal degeneration, demyelination, gliosis and increased functional loss (Fitzgerald et al., 2009; Levkovitch-Verbin et al., 2010). Loss of trophic support due to axonal injury and breakdown of transport systems also negatively impacts the response to injury (Almasieh et al., 2012; Eichler and Rich, 1989; Geden and Deshmukh, 2016; Rich, 1992). From a therapeutic perspective it is clearly important to identify the pathological processes that distinguish primary versus secondary degenerative events after CNS trauma, thereby potentially optimizing treatment regimes.

Partial transection of the dorsal aspect of the optic nerve (ON) in adult rat is an established model that enables the topographic separation of primary versus secondary degenerative events, allowing comparison of the effects of exogenous therapies on retinal ganglion cells (RGCs) in the eye and their axons and associated myelin within the injured central tract (Chiha et al., 2018). Therapeutic injections into the vitreous can directly target cells in the retina and by extension the ON. Further, RGC survival and ON integrity are readily quantitatively assessed using physiological and behavioural methods.

There are numerous examples where exogenously applied neurotrophic factors have been shown to promote neuronal viability and plasticity. These include studies in experimental models of Parkinson's disease (Frim et al., 1994; Kelly et al., 2015), Alzheimer's disease (Jiao et al., 2016), glaucoma (Almasieh et al., 2012; Martin et al., 2003; Nafissi and Foldvari, 2016), brain injury (Chen et al., 2013; Henry et al., 2007), and spinal cord injury (Harvey et al., 2015; Kwon et al., 2007) with many others reviewing this in detail. Complete ON transection initiates RGC death as early as 3 days after injury with 85-90% loss of adult RGCs within 14 days post injury (Berkelaar et al., 1994; Harvey et al., 2006; Isenmann et al., 1997). Similarly, after partial transection (PT) of the dorsal ON, RGCs in dorsal retina directly affected by the injury are dying after 3 days, but cell death overall peaks at 3 months

with evidence of further RGC death 6 months after injury in ventral regions of the retina that are vulnerable to secondary degeneration (Levkovitch-Verbin et al., 2010). Secondary RGC death following PT injury is characterised by necrotic morphologies and multiple mechanisms of apoptosis and death including DNA damage and altered mitochondrial membrane permeability, specifically cytochrome *c* mediated apoptosis (Chiha et al., 2018; Fitzgerald et al., 2009). The survival and regenerative capability of lesioned RGCs can be enhanced to some extent by intraocular injections of recombinant growth factors. For example intravitreal injections of recombinant brain-derived-neurotrophic factor (BDNF) supports compromised lesioned RGCs and promotes their survival (Mansour-Robaey et al., 1994; Mey and Thanos, 1993) However, due to its relatively short half-life, neuroprotection is temporary (Poduslo and Curran, 1996). Repeated intravitreal injections of BDNF or adenovirus vector containing the BDNF gene slightly prolong neuroprotection (Di Polo et al., 1998; Mansour-Robaey et al., 1994), but induce further ocular damage, adverse inflammatory responses, cytotoxicity and transient transgene expression (Harvey et al., 2006; Isenmann et al., 2004; Thomas et al., 2001). In addition, ON injury also results in the downregulation of the high affinity BDNF receptor, tropomyosin-related kinase B receptor (TrkB) in RGCs, 3 to 5 days after injury, thus potentially limiting the neuroprotective duration of BDNF administration during the cell death phase (19). This is overcome by the co-expression of BDNF and its receptor TrkB, which exceeded neuroprotection mediated by either BDNF or TrkB therapy (Osborne et al., 2018).

Therefore, other approaches to enhance injured RGC viability must be explored. A number of studies have now shown that gene therapy using adeno-associated serotype 2 vectors (AAV2) encoding the BDNF gene provides more long-term expression of the peptide, with minimal cytotoxicity and inflammation, promoting the viability of many injured/axotomized RGCs for at least a year (Di Polo et al., 1998; Harvey et al., 2012; Isenmann et al., 2004; LeVaillant et al., 2016; Nafissi and Foldvari, 2016; Osborne et al., 2018; Thomas et al., 2001). The use of bi-*cis*tronic AAV2 vectors encoding both the gene of interest and a fluorescent protein such as green fluorescent protein (GFP) allows the visualisation of transduced RGCs and their axons (6, 12). Other studies have shown the protective potential of inhibiting the phosphorylation of collapsin response mediator protein 2 (CRMP2), a key molecule that binds to and regulates tubulin dynamics and important growth-associated proteins via interaction with kinesin 1 (Kimura et al., 2005). CRMP2 is important in neuronal

polarisation, axonal growth and polymerisation along with the stabilisation of the microtubule assembly during development. Importantly, CRMP2 signalling is directly linked with potent inhibitory effects of myelin on neurite outgrowth and antagonising these signals can regrow neurites through myelin debris substrates following injury (Liz et al., 2014; Nagai et al., 2016). The physiological activity of CRMP2 is inhibited when it is phosphorylated or cleaved in the microtubule-binding domain that includes the Threonine 555 site (Arimura et al., 2005), triggering growth cone collapse and microtubule destabilisation (Yoshimura et al., 2006). Further, the level of phosphorylated CRMP2 is greater in degenerating spinal cord (Nagai et al., 2016) and axons following experimental autoimmune encephalomyelitis (Petratos et al., 2012), while inhibiting CRMP2 phosphorylation demonstrates reparative effects in spinal cord injury (Sekine et al., 2019), by reducing inflammation and enhancing sensitivity to BDNF (Nagai et al., 2016). Moreover, treating RGCs with AAV2 encoding a mutated site-specific T555A CRMP2 gene (AAV2-CRMP2T555A), renders CRMP2 phosphorylation resistant, limiting axonal degeneration and demyelination in murine models of experimental autoimmune encephalomyelitis (Lee et al., 2019; Petratos et al., 2012).

Based on these various observations we have assessed RGC viability, axon maintenance and myelin integrity in response to intravitreally administered AAV2 encoding either BDNF or CRMP2T555A. We have compared the beneficial impact of each of these vectors on directly axotomized neurons versus RGCs with axons that are initially intact but then vulnerable to secondary degeneration. Degenerative events in the cell body and axon can be initiated by different mechanisms, and given that BDNF and CRMP2 may act primarily on cell bodies versus axons respectively (Balastik et al., 2015; Bretin et al., 2005; Chitranshi et al., 2019; Harvey et al., 2012; Lee et al., 2019; Osborne et al., 2018; Petratos et al., 2012; Yuasa-Kawada et al., 2003), thus potentially protecting neuronal integrity at differing neuronal structural and functional domains, intravitreal co-delivery of both AAV2 vectors was also tested to determine if there are any synergistic effects. Morphological and functional analysis was carried out 3 months after unilateral partial dorsal transection of the ON in adult rats. These data are discussed in relation to the different therapeutic profiles of BDNF and CRMP2, as well as the mechanisms involved in primary injury and secondary degenerative events that impact neurons and/or their axons in the CNS.

Materials and Methods

Animals

PVG rats (160-190 g) were obtained from the Animal Resource Centre (Murdoch W.A.) and housed in cages with food and water *ad libitum* and subjected to a standard 12-hour light / dark cycle. All experimental procedures conformed to 'Principles of Laboratory Animal Care' and were approved by the Animal Ethics Committee of The University of Western Australia (approval number RA3/100/673). Animals were euthanized with Euthal (active constituents Pentobarbitone Sodium 170 mg/ml, Phenytoin Sodium 25 mg/ml) 90 days post-surgery; uninjured control animals were euthanized in the same way.

A total of 56 female 8-10-week-old PVG rats was used for these experiments. Animals were allocated to six groups: for immunohistochemistry studies a total of 37 animals was used: normal uninjured (n = 7), AAV2-GFP (n = 7), AAV2-BDNF-GFP (n = 5), AAV2-BDNF (n = 6), AAV2-CRMP2T555A-GFP (n = 6), AAV2-BDNF plus AAV2-CRMP2T555A-GFP (n = 6). The bi-*cis*tronic AAV2-BDNF-GFP and AAV2-BDNF groups were pooled. Nineteen rats were used for the electron microscopy (EM) studies: normal uninjured (n = 4), AAV2-GFP (n = 4), AAV2-BDNF-GFP (n = 1), AAV2-BDNF (n = 3), AAV2-CRMP2T555A-GFP (n = 3), AAV2-BDNF plus AAV2-CRMP2T555A-GFP (n = 4). The AAV2-BDNF-GFP and AAV2-BDNF groups were pooled.

Intravitreal injections

Rats were anesthetized with ketamine (50 mg/kg)/ xylazine (10 mg/kg, Troy Laboratories, NSW, Australia) administered intraperitoneally. Intravitreal AAV2 eye injections (each 4 µl in volume) were carried out 10 days prior to PT surgery using a glass micropipette inserted through the sclera as described previously (Harvey et al., 2002). The AAV2-GFP vehicle control and AAV2-BDNF-GFP (8×10^{12} GC/ml) vectors were generated from pTRUF12 (GTC Virus Vector Core, NC) backbone and obtained from Gene Therapy Center Virus Vector Core Facility (University of North Carolina, Chapel Hill, NC), AAV2-BDNF (8×10^{12} GC/ml) was generated from pTRUF12.1 plasmids (donated by Joost Verhaagen, Amsterdam, Netherlands). The construction of rAAV-flag-CRMP2T555A-GFP (2.1×10^{13} GC/ ml) plasmids generated through Vector BioLabs was as described previously (Lee et al.,

2019; Petratos et al., 2012). In the bi-*cis*tronic vectors, BDNF and CRMP2T555A were both linked via an internal ribosome entry site (IRES) to GFP.

Partial transection of the optic nerve

Unilateral PT of the ON was performed as previously described (Fitzgerald et al., 2010; Fitzgerald et al., 2009; Martin et al., 2003). Briefly, PVG rats were anaesthetized with ketamine (50 mg/kg) and xylazine (10 mg/kg, Troy Laboratories, NSW, Australia) administered intraperitoneally. An incision was made in the skin overlying the right eye and the underlying connective tissue incised by blunt dissection to expose the back of the eye. Lachrymal glands were deflected and extra ocular muscle incised to access the nerve. A 200-µm incision was made on the dorsum of the optic nerve approximately 1 mm behind the optic nerve head using a diamond keratotomy knife (Geuder, Germany). Post-operative analgesia (2.8 mg/kg carprofen, Norbrook Australia, Pty. Ltd., VIC, Australia) and 1 ml sterile PBS were administered subcutaneously and animals recovered on a warming blanket. Uninjured, age-matched animals were used as controls, as we have previously demonstrated no significant differences between sham-operated and normal animals in relevant outcomes including RGC numbers (Fitzgerald et al., 2009).

Optokinetic responses

The uninjured left eye was closed with 6-0 silk suture under anaesthesia as detailed above, one day prior to behavioural testing. Eyelid suture ensured that all responses were due to the visual ability of the experimental eye following partial ON transection. Optokinetic nystagmus is an accepted first-line screening test of visual function, and was conducted as described previously (Abdeljalil et al., 2005; Fitzgerald et al., 2009). A normal optokinetic nystagmus comprises a smooth pursuit, with the head moving at the same speed as stripes inside a rotating drum, followed by a rapid realignment movement or fast reset phase (Fig. 1A-B). The smooth pursuit and fast reset phases were analysed separately by a single investigator blinded to the treatment identity of the animals. Numbers of responses were analysed using one-way analysis of variance (ANOVA), and Dunnett's *post-hoc* test (significance value $p \leq 0.05$). Analyses were performed by counting the number of purposeful movements in the direction of the stripes within the period each rat was engaged in the task.

Immunohistochemistry

Experimental animals were sacrificed 3 months post injury and perfused transcardially with saline followed by 4% paraformaldehyde (Sigma-Aldrich; St. Louis, Missouri, USA) in 0.1M phosphate buffer, pH 7.2; uninjured control animals were processed similarly. The eyes and attached ONs were post-fixed in 4% paraformaldehyde overnight, cryoprotected by immersion in 15% sucrose in PBS, before they were embedded in optimal cutting temperature (OCT) compound (Sakura Finetek, USA). The retinae and ONs were cryosectioned (20µm and 14 µm respectively) longitudinally along the dorsal/ventral axis. If not processed immediately, the slides were stored at -80ºC. Retinal and ON sections were air dried for 1 hour at room temperature, rehydrated in PBS, and incubated overnight at 4ºC in combinations of primary antibodies were blocked in 5% normal donkey serum (NDS) and sterile PBS+0.2% Triton X100. Primary antibodies used for immunohistochemical assessment were: rabbit GFP (1:400; Chemicon); mouse βIII-tubulin (1:1000; IgG2A, Covance), goat Brn3A (1:400, Santa Cruz Biotechnology), rabbit Caspr (1:500, Abcam), goat Iba1 (1:1000, Abcam), rabbit 4-hydroxynonenal HNE (1:400, Abcam). Antibody binding was visualized following 2-hour incubation at room temperature with appropriate Alexa Fluor 488, 555 and 647 secondary antibodies (1:400; Molecular Probes, Life technologies) and Hoechst nuclear stain (0.5µl/ml, Invitrogen, Scoresby, Victoria, Australia). Slides were washed in PBS and cover-slipped using Fluoromount-G (Southern Biotechnology).

Confocal microscopy and immunohistochemical analysis

Retinal and ON sections were imaged with a Nikon A1Si confocal microscope using a 60 × oil immersion objective or 20x objective. Samples were simultaneously excited with 405 nm and 488 nm lasers and fluorescence emission detected using the spectral detector over the range 410 nm to 600 nm with a 10 nm grating resolution and either 8- or 16-line averages. Fluorescent probes were spectrally unmixed in Nikon NIS Elements software (version 4.20) using single label control samples for reference spectra. Z stacks were collected at 0.5µm slice intervals through the entire section thickness and maximum intensity projections prepared for presentation. For semi-quantification of immunofluorescence in longitudinal ON sections, ON were visualised and Z stacks prepared at 20x magnification. Image analysis was performed on the ventral ON below the injury site using FIJI analysis software setting constant arbitrary threshold intensities for each image, and semi-quantifying mean intensities

and areas above the set threshold. Immunointensity data were normalised to background within the same section to adjust for variations in section thickness and staining application.

Quantification of RGC survival and transduction efficiency

Retinal sections were imaged as detailed above using the 60x objective with oil immersion and analysed by an operator blinded to experimental groups. βIII-tubulin immunoreactivity surrounding a Hoechst labelled nucleus and $Brn3A^+$ immunohistochemistry were used as markers for RGCs in the ganglion cell layer as described previously (Fitzgerald et al., 2009; Nadal-Nicolas et al., 2012; Nadal-Nicolas et al., 2009). $βIII\text{-}tubulin^+$ and $Brn3A^+$ RGCs were counted in 20µm thick dorso-ventral radial sections of the retina, in three fields of view along linear regions of the dorsal, central and ventral retina. RGC counts were made using the optical fractionator method as described previously (Fitzgerald et al., 2009; Gundersen, 1986; Mead et al., 2014) and RGC per mm^2 estimates were made using the thickness of the sections (20µm) and the linear length of the field of view.

Node paranode analysis

For node/paranode analyses, images of longitudinal ON sections were captured using a 60x objective with oil immersion, and ~100 node/paranode complexes were assessed from a single defined and consistent field of view visualised in a single in focus slice from a z-series of images, collected as described above, in ventral ON below the injury site. The length of the paranodal gap, was defined as the distance between two $Caspr^+$ paranodes and the paranodal length was defined as the average length of the flanking $Caspr^+$ paranodes. Assessments of $βIII\text{-}tubulin^+$ complexes were only conducted when a βIII-tubulin+ axon was flanked by two $Caspr^+$ paranodes. Assessments were conducted by a single investigator blinded to group identity.

Electron microscopy: Tissue preparation, Image collection and analysis

Ultrastructural analysis was undertaken for 3 to 4 animals per group. Following euthanasia, animals were transcardially perfused with 0.9% saline followed by phosphate buffered 2.5% glutaraldehyde (Sigma-Aldrich: St Louis, Missouri, United States). The ON containing the injury site was post-fixed in 1% osmium (ProSciTech, Kirwan, Queensland, Australia) for 90 min with shaking, and processed using a Lynx tissue processor into Araldite Procure mixture (ProSciTech). Embedded ON segments were cured for 24 h, serially cross-sectioned

(1µm) in three sets at 50µm intervals, and stained with toluidine blue to identify the injury site. Ultrathin sections were also cut, and low-power photographs of entire sections were taken to ensure identification of the lesion site. Sequential high-power images were captured at 4000× magnification with 15-20% overlap from ventral ON sections. The images were saved as TIF files, stitched together using the MosaicJ plugin (FIJI) and all axons within the image were assessed using FIJI analysis software to determine the minimum axon diameter, axon area, and the minimum fibre diameter (i.e., including both the axon and the myelin sheath). G ratios were calculated by dividing the minimum diameter of each axon by the minimum diameter of the fibre, including both the axon and the myelin sheath of normally myelinated axons.

Statistical analyses

Results were analysed using the statistical package Graphpad prism (version 8.00 GraphPad Software, La Jolla California USA). Equality of variance F-tests were conducted to test for homogeneity of variance in groups within experiments. All data achieved normal distribution. All data are expressed as means of each treatment group ± SEM, unless otherwise stated. ANOVAs followed by Tukey post hoc test was used to statistically compare quantitative measures of each treatment group to all other treatment groups. For selected outcomes of interest, comparisons were made to injured AAV2-GFP control using Dunnett's post hoc tests. ANOVA F-test and degrees of freedom (df), as well as p value from post hoc tests are given. All statistical tests required $p \leq 0.05$ for significance. For almost all statistical comparisons the AAV2-BDNF-GFP and AAV2-BDNF treatment groups were not significantly different from each other, and the data from these two groups were therefore pooled. Based on this, pooling was also extended to the EM data even though only one animal was analysed from the AAV2-BDNF-GFP treatment group. No outliers were removed.

Results

Transgene expression in the retina and optic nerve of AAV2-injected eyes

Using AAV2 as a vector for gene transduction is associated with a delay in activation and expression of the transgene due to the time needed for second strand synthesis, transcription and subsequent translation (Fisher et al., 1996; Leaver et al., 2006). Some transgene expression has been demonstrated as early as 3 days post-injection (Sarra et al., 2002),

however in another study significant levels of expression were not observed until 7 days after intraocular administration (Harvey et al., 2002). Based on these data we chose to inject the AAV viral constructs 10 days prior to partial ON transection, to ensure significant levels of functional therapeutic constructs at the time of injury. Note that previous studies have shown that transduction of RGCs with these same AAV2 vectors allows efficient target gene transfer, regulating the overexpression of both mRNA transcripts, respectively. For instance, immunohistochemistry was used to show BDNF expression in transduced RGCs (Leaver et al., 2006) along with immunohistochemistry and immunoprecipitation using antibodies specific for the C-terminus of CRMP2 to demonstrate altered phosphorylated and unphosphorylated CRMP2, as well as modulation of key binding proteins such as tubulin and kinesin (Lee et al., 2019; Petratos et al., 2012).

Three months following ON injury, retinal and ON tissue from rats injected intravitreally with AAV2-GFP, AAV2-BDNF-GFP, AAV2-BDNF, AAV2-CRMP2T555A-GFP or combined AAV2-BDNF and AAV2-CRMP2T555A-GFP was harvested. Post-IRES GFP expression was detected immunohistochemically and quantified when co-localised with βIII-tubulin$^+$ RGCs in the ganglion cell layer (Supplementary Fig. 1A-D). Based on this GFP expression, the average retinal transduction efficiency of βIII-tubulin$^+$ RGCs was 40.9±1.75% SEM transduction following AAV2-BDNF-GFP injections, 40.4±1.9% SEM following AAV2-CRMP2T555A-GFP injections and 43.9±1.3% SEM following combined AAV2-BDNF and AAV2-CRMP2T555A-GFP injection (Supplementary Fig. 1A). Transduction efficiency was not statistically different between the groups in dorsal and ventral retina ($p \geq 0.05$), however in central retina combined AAV2-BDNF plus AAV2-CRMP2T555A-GFP transduction was significantly higher ($p = 0.02$) than AAV2-BDNF alone. This rate of transduction (about 40%) is remarkably similar to that found previously using both AAV2-GFP and AAV2-CRMP2T555A-GFP vectors (Petratos et al., 2012).

The anterograde transport of intravitreally delivered post-IRES GFP was visualised along the ON following PT injury (Supplementary Fig. 1). Assessing ON transfection using immunohistochemistry to detect GFP and semi-quantifying outcomes as area above set threshold, we identified no statistical difference between intravitreal injection of AAV2-BDNF-GFP, AAV2-CRMP2T555A-GFP and combined AAV2-BDNF plus AAV2-CRMP2T555A-GFP. We also observed co-labelling of viable GFP and βIII-tubulin$^+$ axons in

the ON (Supplementary Fig. 1G-H), suggesting intact axonal transport systems in transduced RGCs (Lee et al., 2019; Petratos et al., 2012; Sekine et al., 2019; Yoshimura et al., 2006).

AAV injections and the effect on visual function following partial ON transection

As has been previously reported, partial ON transection resulted in a significant reduction in the number of optokinetic nystagmus responses measured 3 months after PT (Payne et al., 2012; Savigni et al., 2013; Selt et al., 2010; Szymanski et al., 2013). We did not observe statistically significant reductions in the number of total pursuits (smooth, partial and micro pursuits) between normal uninjured animals and injured animals treated with AAV2-GFP, however treatment groups that include BDNF namely, AAV2-BDNF and treatment that combines AAV2-BDNF plus AAV2-CRMP2T555A-GFP, significantly increased the total number of pursuits ($p = 0.04$ and 0.03 respectively, $F = 3.00$ (DF 41), Fig. 1C) compared to AAV2-GFP. The number of smooth pursuits and fast rests was not significantly different between the treatment groups ($p > 0.05$ $F = 1.10$, (DF 43), $F = 1.41$ (DF 40) respectively, Fig. 1D-E).

RGC viability after partial optic nerve transection

Three months after partial ON transection the number of viable RGCs was assessed in retinal sections using βIII-tubulin$^+$ and Brn3A$^+$ immunohistochemistry (Fig. 2A,D) (Nadal-Nicolas et al., 2009). RGC numbers were quantified in three regions of the retina: dorsal retina, impacted by primary degenerative mechanisms; central retina vulnerable to mechanisms of primary and secondary degeneration; and ventral retina vulnerable predominantly to secondary degeneration (Fig 1A) (Fitzgerald et al., 2009). Further, given that not all RGC subtypes express Brn3A and RGC loss after injury is often preceded by a downregulation in Brn3A (Nadal-Nicolas et al., 2012; Nadal-Nicolas et al., 2009), the total Brn3A expression was compared between different treatment groups as a proportion of the total number of βIII-tubulin$^+$ RGCs (Fig. 2E).

Analysis of the estimated number of βIII-tubulin$^+$ RGCs/mm^2 in dorsal retina revealed a significant 60% decrease in the number of surviving RGCs after control intravitreal AAV2-GFP injections ($p = 0.01$, $F = 1.24$ (DF 86), Fig. 2F) 3 months after partial ON transection. Treatment with AAV2-BDNF in particular resulted in a moderate increase in RGC viability

(Leaver et al., 2006), but this increase was not found to be significant. Similar changes in viable RGC numbers were observed using $Brn3A^+$ as the RGC marker, although overall numbers were of course lower.

In central retina, compared to normal retina, RGC density decreased significantly by about 60-70% following partial ON transection and AAV2-GFP treatment using either βIII-tubulin$^+$ ($p = 0.0002$, $F = 1.24$ (DF 86), Fig. 2G) or $Brn3A^+$ ($p = 0.0005$, $F = 1.30$ (DF 80)) quantification respectively. Treatment with intravitreally administered viral vectors resulted in significant increases in the number of RGCs/mm^2 in central retina ($p \leq 0.01$, Fig. 2G). Using βIII-tubulin$^+$ estimates, injections of AAV2-BDNF, AAV2-CRMP2T555A-GFP and AAV2-BDNF plus AAV2-CRMP2T555A-GFP increased the number of RGCs to approximately 97, 89 and 97% of normal values respectively. Interestingly, using $Brn3A^+$ quantification, only AAV2-CRMP2T555A-GFP and the combination of AAV2-BDNF and AAV2-CRMP2T555A-GFP resulted in statistically significant increases in RGC numbers ($p \leq 0.05$, $F = 1.30$ (DF 80)).

In ventral retina, after AAV2-GFP injections the relative number of RGCs decreased significantly ($p \leq 0.05$, $F = 1.24$ (DF 86)) and ($p \leq 0.05$, $F = 1.30$ (DF 80)) to about 40% and 25% of control values using βIII-tubulin$^+$ and $Brn3A^+$ estimates respectively (Fig. 2H). After partial ON injury, in all AAV regimes the estimate of viable RGC number was higher than in the AAV2-GFP group, however only the treatment with AAV2-BDNF resulted in a saving of RGCs at the $p \leq 0.05$ significance level (Tukey post hoc test). The difference between the AAV2-BDNF and AAV2-CRMP2T555A-GFP group just failed to reach significance ($p = 0.055$).

Transduction of RGCs with AAV2 administered viral constructs limits axonal degeneration

Having established that intravitreally administered AAV2-BDNF, AAV2-CRMP2T555A-GFP and a combination of the two is associated with the protection of many compromised RGCs, we then addressed whether this neuroprotection is associated with preservation of axons in the ON (Fig. 3). Using EM, axonal density was assessed in transverse sections of ventral ON (area below blue dotted line in Fig. 3B) 3 months after dorsal transection injury. The number of axons per mm^2 decreased significantly ($p \leq 0.0001$, $F = 30.16$ (DF 12), Fig 3A) following partial ON injury and AAV2-GFP treatment compared to normal uninjured

animals (Fig. 3E, F). Intravitreal injection of AAV2-BDNF or AAV2-CRMP2T555A-GFP significantly ($p = 0.0001$) restored the number of axons to about 90% of normal, and the combination of AAV2-BDNF and AAV2-CRMP2T555A-GFP preserved densities to about 97% of normal ($p \leq 0.0001$, $F = 30.16$ (DF 12), Fig. 3G)). Statistical analysis using Tukey's rather than Dunnett's test revealed a statistically significant decrease in axonal counts in the AAV2-BDNF versus normal group ($p = 0.026$).

These axonal counts from transverse EM sections were closely mirrored using semi quantitative immunohistochemical analysis of βIII-tubulin$^+$ axonal profiles in longitudinal ON sections (Fig.3 C, D). There was a significant decrease in βIII-tubulin$^+$ immunointensity following injury ($p = 0.01$, $F = 11.60$ (DF 27) Fig. 3C), while treatment with AAV2-BDNF, AAV2-CRMP2T555A-GFP and AAV2-BDNF + AAV2-CRMP2T555A-GFP resulted in significant increases in βIII-tubulin$^+$ immunointensity ($p = 0.008$, $p = 0.0001$ and $p < 0.0001$ respectively, $F = 11.60$ (DF 27)). In order to ensure changes to axonal density were not a result of ON swelling of shrinkage, ON diameter and area of ventral ON was measured and was found not be significantly different in injured and treated animals compared to normal uninjured animals ($p \geq 0.05$, $F = 0.12$ (DF 14) and $F = 0.39$, (DF 14) respectively Fig. 3K-M). Tukey's test revealed a significant difference between the βIII-tubulin$^+$ fluorescence intensity in the ON of AAV2-BDNF versus AAV2-CRMP2T555A-GFP groups ($p = 0.023$).

RGC transduction with AAV2 viral vectors limits structural disruptions of the node of Ranvier complex

Structural parameters of the nodes of Ranvier and of paranodes were quantified in ventral ON following PT injury, and the effects of intravitreally administered viral constructs quantitatively assessed (Fig. 4). It has been previously demonstrated in this injury model that the paranodal gap, defined as two Caspr+ paranodes, not necessarily with βIII-tubulin$^+$ immunoreactivity between, increased significantly 3 months following partial ON injury (Giacci et al., 2018; Szymanski et al., 2013). Similarly, in this study we demonstrated significant increases in the length of the paranodal gap with injury when the paranodal gap was defined in this way ($p = 0.005$, $F = 4.97$ (DF 28), Fig. 4A, C). The combination of intravitreally administered AAV2-BDNF and AAV2-CRMP2T555A-GFP restored the paranodal gap to normal parameters ($p = 0.008$). However, when we limited paranodal gap analysis to βIII-tubulin$^+$ axons flanked by Caspr$^+$ paranodes, which represents a more rigours

definition of the Node of Ranvier, we observed a significant decrease ($p \leq 0.001$, $F = 5.69$ (DF33), Fig. 4B,D, E) in the paranodal gap following injury when compared to normal uninjured animals. Only intravitreal treatments that included AAV2-BDNF restored the paranodal gap to normal parameters; AAV2-BDNF ($p=0.02$, $F = 5.69$ (DF33)) and AAV2-BDNF plus AAV2-CRMP2T555A-GFP ($p=0.008$, $F = 5.69$ (DF33)). Analysis of the percentage of βIII-tubulin$^+$ node/paranode complexes over total node/paranode complex was approximately 82 ±1.97% in normal uninjured animals, which decreased significantly ($p = 0.001$, $F = 6.627$ (DF 29) to an average of 69 ± 2.37% following partial ON transection, data not shown. Treatment with the viral vectors that include AAV2-BDNF significantly restored the percentage of βIII-tubulin$^+$ node/paranode complexes to normal levels; specifically AAV2-BDNF injections significantly increased the complex composition to 82 ± 1.07% ($p = 0.0005$, $F = 6.627$ (DF 29)) and the combination of AAV2-BDNF and AAV2-CRMP2T555A-GFP increased the percentage of βIII-tubulin$^+$ node/paranode complexes to 79 ± 2.1%9 ($p = 0.01$), while AAV2-CRMP2T555A-GFP alone resulted in no statistically significant change (77 ±2.24%).

The proportion of atypical node/paranode complexes, composed predominantly of hemi-nodes and single nodes, increased significantly ($p \leq 0.0001$, $F = 16.01$ (DF 28), Fig. 4G) from 21 ± 0.85% in normal uninjured animals to 41 ± 2.52% in injured animals injected with AAV2-GFP. The percentage of atypical node/paranode complexes was preserved ($p \leq 0.0001$, $F = 16.01$ (DF 28)) following intravitreal injections of AAV2-BDNF, AAV2-CRMP2T555A-GFP and combined AAV2-BDNF plus AAV2-CRMP2T555A-GFP (Fig. 4G). Consistent with these data, the proportion of typical node/paranode complexes was significantly decreased following injury ($p = 0.01$, $F = 4.71$, (DF 31), Fig. 4H). Treatment with the three therapeutic viral vector combinations maintained the proportion of typical complexes within normal parameters. This was associated with a significant increase in the proportion of hemi-nodes (Fig. 4K) following partial ON injury and AAV2-GFP injections ($p < 0.0001$, $F= 15.58$ 9 (DF 31), Fig 3I), and maintenance of a near normal proportion of hemi-nodes after all AAV treatments ($p < 0.0001$). Assessment of the proportion of single nodes showed a significant increase with injury compared to uninjured normal animals ($p = 0.04$, $F = 2.49$ (DF31)), however treatment with the BDNF and CRMP2T555A vectors did not significantly influence this parameter (Fig. 3J).

RGC transduction with viral vectors and the effect on G-ratio, myelin thickness and myelin decompaction

G-ratio is the ratio of the inner axonal diameter to the total outer diameter and is used as an assessment of axonal myelination and, by inference, axonal conduction (Chomiak and Hu, 2009). Relative to normal animals, G-ratio increases 3-months following partial ON injury have previously been demonstrated (Payne et al., 2012). This was confirmed in our study with a statistically significant increase in mean G-ratio ($p = 0.02$, $F = 6.3$ (DF 15), Fig. 5A) 3-months following ON injury and AAV2-GFP injection. Intravitreal treatments with AAV2-BDNF and AAV2-CRMP2T555A-GFP significantly reduced the G-ratio ($p \leq 0.02$). Similarly, we confirmed previously observed decreases in myelin thickness after partial ON injury ($p = 0.02$, $F = 3.71$ (DF 15)), while intravitreally delivered therapeutic factors increased myelin thickness relative to the AAV2-GFP treatment (Fig. 5B). The relative frequency distribution of the diameters of axons with normal levels of myelin decompaction (0-15% levels of decompaction) illustrates that there was no change in the distribution of these axon diameters following injury or intravitreal AAV2-BDNF and/or AAV2-CRMP2T555A-GFP treatments (Fig. 5C).

The conduction velocity of action potentials is directly proportional to the degree of myelination, and myelin decompaction leads to suboptimal conduction velocity (Gutierrez et al., 1995; Waxman, 1980). The proportion and degree of myelin decompaction was assessed and axons with myelin decompaction between 0 to 15% of fibre circumference were categorised as normally myelinated axons. The second and third categories included axons with myelin decompaction between 20 and 30% and over 30% of fibre circumference respectively (Fig. 5D-G). Following partial ON transection, the percentage of axons with decompaction up to 15% of fibre circumference decreased significantly ($p \leq 0.0001$, $F = 33.69$ (DF 39)). Treatment with viral vectors significantly attenuated the myelin decompaction ($p<0.0001$, $p=0.0004$, $p=0.005$). This was observed following individual intraocular injection of AAV2-BDNF or AAV2-CRMP2T555A-GFP, or injection with the combination of AAV2-BDNF and AAV2-CRMP2T555A-GFP, respectively. The proportion of axons with myelin decompaction between 20-30% of fibre circumference significantly increased ($p \leq 0.0001$, $F = 33.69$ (DF 39)) following ON injury, and only treatment with AAV2-BDNF maintained the proportion of decompacted axons ($p \leq 0.0001$).

The relationship between myelin thickness and axonal calibre also influences conduction velocity (Waxman, 1980) and it is therefore of interest that we observed changes in the correlation between the two measures as a consequence of partial ON injury and various AAV2 treatments (Fig. 5H). The relationship between axon diameter and myelin thickness is depicted using linear regression, where R^2 values are between 0.0 and 1.0, with higher values indicating direct relationship between axon size and myelin thickness. In normal uninjured animals, the correlation between myelin thickness and axon diameter had an $R^2 = 0.42$, which was reduced to $R^2 = 0.20$ after ON injury. Treatment with AAV2-BDNF restored the correlation between myelin thickness and axon diameter to $R^2 = 0.31$. Treatment with AAV2-CRMP2T555A-GFP resulted in $R^2 = 0.005$ correlation between myelin thickness and axonal diameter, while the combined AAV2 treatment yielded an $R^2 = 0.0002$.

RGC transduction with viral vectors reduces oxidative stress but not inflammatory cell markers in the ON

The oxidative stress marker HNE has been demonstrated to increase in ON vulnerable to secondary degeneration (O'Hare Doig et al., 2017). Similarly, we demonstrated that HNE was significantly increased in ventral ON areas ($p = 0.002$, $F = 5.53$ (DF 27), Supplementary Fig. 2A-D). Only treatment with a combination of AAV2-BDNF and AAV2-CRMP2T555A-GFP significantly reduced HNE immunoreactivity relative to injury ($p = 0.02$). The marker of resident microglia, Iba1, was also significantly increased in ventral ON 3 months following injury ($p = 0.04$, $F = 1.85$ (DF 27), Supplementary Fig. 2E-H), but was unaffected by the treatment protocols ($p \geq 0.05$).

Discussion

The present results show that, three months after partial ON transection, secondary degenerative events in the retina and nerve are attenuated long-term by therapeutic administration of AAV vectors encoding either BDNF or a mutant, phospho-resistant CRMP2 (CRMP2T555A). Intravitreal administration of AAV2-BDNF, AAV2-CRMP2T555A-GFP, or the combination of the two constructs significantly enhanced the survival of βIII-tubulin$^+$ RGCs in central retina, while in ventral retina in which RGCs were vulnerable to secondary degeneration, only AAV-BDNF was effective. Most (but not all) measured components of axonal and myelin structure were also preserved following

intravitreal administration of AAV2-BDNF, AAV2-CRMP2T555A-GFP and when combined. Furthermore, in combination these therapeutics were associated with a reduction in oxidative stress events. An improvement in some aspects of visual function was also recorded when AAV-BDNF vectors were used.

The efficacy of AAV mediated therapeutic intervention has not previously been assessed on secondary degenerative events in the injured visual system. A limitation in the administration of AAV vectors is the time delay between ocular administration and transgene expression (Harvey et al., 2002; Leaver et al., 2006; Petratos et al., 2012; Sarra et al., 2002). In the present study, intravitreal AAV injections were performed 10 days prior to ON surgery. We previously demonstrated transgene expression at 3 and 7 days post ocular administration (Harvey et al., 2002), and vector expression gradually increases in a time dependant manner (Igarashi et al., 2016). Thus 10 days was sufficient to ensure availability of each therapeutic transgene product when the partial ON injury was performed. Such an approach may limit the clinical applicability of AAV for CNS trauma, however supplementary trophic factor injections can be used as a temporary but supportive subsidiary strategy (Koeberle and Ball, 2002; Mansour-Robaey et al., 1994; Mey and Thanos, 1993), particularly when combined with AAV delivery at the time of injury (Hellstrom et al., 2011).

RGC viability after partial ON injury

The extent of neuronal survival after an injury is in many instances linked to the level of therapeutic viral vector transduction. Given that this study aimed to examine the therapeutic efficacy of intravitreally administered viral vectors on RGCs vulnerable to secondary degeneration after dorsal ON transection, the AAV injections were targeted towards the ventral quadrant of the retina to maximise transduction efficiency. Nonetheless we found no measurable differences in the level of RGC transduction in dorsal, central or ventral retina and levels of transduction were similar for all vectors. The importance of transduction efficiency depends to some extent on whether the vector-mediated product is secreted from transduced cells. Thus the therapeutic effects of CRMP2T555A are likely to be more limited to the transduced RGC population, whereas it is known that the survival of non-transduced RGCs after AAV-BDNF delivery is enhanced via the release of the neurotrophin from nearby transduced cells, thereby providing paracrine or bystander support (Baumgartner and Shine,

1997; Leaver et al., 2006). In addition, it should be noted that the survival of apparently non-transduced RGCs may also reflect lower post-IRES expression of the GFP transgene in some neurons (Mizuguchi et al., 2000).

The trophic effect of recombinant AAV2-BDNF is likely mediated through vector translation followed by the release of functional BDNF protein into the extracellular environment, which enables it to bind to the RGC surface TrkB receptors (Hellstrom et al., 2011). This results in receptor dimerization and autophosphorylation, and the activation of several intracellular signalling cascades that modulate growth-associated genes, enhance plasticity, and support the survival of existing neurons (Huang and Reichardt, 2001; Tejeda and Diaz-Guerra, 2017). Furthermore, via PI3K and Akt pathways, BDNF can also inhibit GSK3β activity, acting to reduce potential CRMP2 phosphorylation (Namekata et al., 2012).

The therapeutic effect of intravitreally administered AAV2-CRMP2T555A-GFP involves the translation of the functional phospho-resistant CRMP2 protein, which is then transported along the axon (Liz et al., 2014; Nagai et al., 2016). In neurons, CRMP2 binds to tubulin heterodimers and promotes microtubule assembly, however the phosphorylation of CRMP2 significantly attenuates that binding affinity (Fukata et al., 2002). Many factors can influence the phosphorylation status of CRMP2 (Yamashita and Goshima, 2012) but it is worth noting here that adult RGCs express a number of class 3 semaphorins as well as cognate plexin and neuropilin receptors (de Winter et al., 2004), and expression levels of many of these semaphorins are altered by ON injury (Sharma et al., 2012). Signal transduction of ligated Plexin A2 receptor, in collaboration with NgR1 has been identified to regulate the phosphorylation of CRMP2 in regenerating axons limiting their growth after injury (Sekine et al., 2019). In addition, phosphorylated-CRMP2 interacts with and increases the membrane insertion of voltage gated sodium and calcium channels (Brittain et al., 2012; Chew and Khanna, 2018), with subsequent intracellular calcium dysregulation identified as key secondary degenerative mechanisms governing partial ON transection (O'Hare Doig et al., 2017). Indeed, the overexpression of CRMP2 has been shown to significantly delay axonal retraction bulb formation, temporarily rescuing mitochondrial transport defects after axotomy and attenuating axonal fragmentation following ON crush injury (Kinoshita et al., 2019; Kondo et al., 2019; Zhang et al., 2007). Similarly, significant protection of axons and myelin was observed by targeting GSK3β activity or inhibiting Nogo-A and thus limiting CRMP2

phosphorylation (Inagaki et al., 2001; Leibinger et al., 2017; Petratos et al., 2012; Sekine et al., 2019; Wilson et al., 2012). Additionally, delivery of the AAV2-CRMP2T555A vector has been demonstrated to prevent axonal degeneration, demyelination and ameliorate clinical progression in a murine ON model of multiple sclerosis (Petratos et al., 2012) illustrating the importance in abrogating the downstream phosphorylation of CRMP2 for axo-myelin integrity. Together it seems likely that RGC survival following the administration AAV2-CRMP2T555A-GFP is mediated by maintaining the integrity of the axonal cytoskeletal structure, and perhaps by stabilising calcium homeostasis.

Intravitreal injections of AAV2-BDNF, AAV2-CRMP2T555A-GFP, and both vectors together protected the number of surviving RGCs to varying degrees, depending on retinal location. In the central retina, where the impact of primary and secondary degenerative mechanisms is both present all three treatment regimens were effective in maintaining βIII-tubulin^{+} RGCs. Not all RGCs express Brn3A, and injury can result in downregulation of this transcription factor (Nadal-Nicolas et al., 2012; Nadal-Nicolas et al., 2009), ; it is therefore intriguing that only AAV2-CRMP2T555A-GFP and the combination of AAV2-BDNF and AAV2-CRMP2T555A-GFP resulted in statistically significant increases in Brn3A^{+} RGC numbers in central retina.

In the ventral retina, where cell loss is predominantly due to secondary degeneration, all treatments showed a trend towards enhanced survival, but only AAV2-BDNF was significantly neuroprotective when compared to AAV2-GFP controls. Surprisingly, the addition of AAV2-CRMP2T555A-GFP attenuated the neuroprotective capacity of AAV2-BDNF in the combined AAV regime, even though there is enhanced TrkB transport and BDNF-mediated signal transduction in CRMP2-bound microtubules (Arimura et al., 2009b; Nagai et al., 2016; Sekine et al., 2019). It remains unclear why treatments that include CRMP2 are only partially effective against mechanisms of RGC demise in response to secondary degeneration. Enhanced retrograde and anterograde axonal transport and microtubule stability, as a consequence of CRMP2 interactions with kinesins (Sekine et al., 2019) and tubulin, are likely to mediate somatic neuroprotection observed in the central retina (Arimura et al., 2009a; Kimura et al., 2005), yet one might have expected enhanced viability of RGCs in the ventral retina due to better maintenance of retrograde systems transporting endogenous neurotrophins such as BDNF from central visual targets in the brain (Quigley et al., 2000).

RGC axons and myelin integrity in the partially injured optic nerve

In the present study, three months after partial dorsal transection, and generally consistent with the observed increase in RGC survival, all AAV vector regimens resulted in statistically significant maintenance of axonal density in the ventral portion of the ON. All treatments (AAV2-BDNF, AAV2-CRMP2T555A-GFP and AAV2-BDNF plus AAV2-CRMP2T555A-GFP) significantly protected RGCs when combining counts of βIII-tubulin^{+} RGCs in central and ventral retina (Supplementary Fig. 3), closely reflecting ON axon counts. The inconsistency between ventral RGC and axonal counts is potentially due to a misalliance between regions of tissue sampling as secondary degeneration encompasses large areas of the retina and ON. To unequivocally determine the association between ventral located RGCs and axons, tracing individual axons to their source somata, will provide insight (Luo et al., 2013). However, as discussed above, it is also apparent that ocular administration of mutant CRMP2T555A, while enhancing stability of vulnerable axons, is less effective in suppressing cell death programs in ventrally located RGCs vulnerable to secondary degeneration. We have previously demonstrated a delay in the degenerative sequence of secondary degeneration (Chiha et al., 2018); the pre-emptive treatment with phospho-resistant CRMP2T555A may inadvertently disrupt cytoskeletal dynamics and axonal transport and induce microtubule hyper-stability in unaffected axons and thus potentially negatively impact ventral RGCs. Thus, in other conditions, hyper-stability of microtubules is thought to induce degenerative events and can be detrimental to overall neuronal health (Dubey et al., 2015; Evans et al., 2005).

An increase in the length of the node of Ranvier has been implicated in numerous CNS pathologies (Giacci et al., 2018; O'Hare Doig et al., 2017; Szymanski et al., 2013). Consistent with previous studies (Szymanski et al., 2013), we observed changes in the paranodal gap three-months following partial ON transection and only treatment that combined the therapeutic benefits of AAV mediated expression of BDNF and phospho-resistant CRMP2 was effective at preservation of structure. The lengthening of the paranodal gap is arguably due to myelin retraction and detachment of paranodal loops (Fu et al., 2009; Popko, 2000). The physiological implication of paranodal gap lengthening is associated with conduction alterations. Studies have demonstrated increased nodal surface area is associated with increased conduction when combined with increased Na_v (voltage gated sodium channels)

density, however conduction velocity decreases, if Na_v density does not increase (Moore et al., 1978). Although we did not directly measure conduction velocity in secondary degeneration, given that others have previously demonstrated a progressive decrease in conduction velocity following ON lesion (Wang et al., 2012), we can extrapolate that a diminution in Na_v occupied nodal space, was a contributor to functional impairment. Intriguingly, in the subset of node/ paranode complexes where the axon is βIII-tubulin$^+$ immunopositive and flanked by Caspr labelled paranodes, which represents a rigours definition of the Node of Ranvier, the paranodal gap decreased in axons vulnerable to secondary degeneration. Similar decreases were also observed following chronic stress in mice, where the structure and clusters of Na_v were preserved (Miyata et al., 2016). The current data and other studies suggest the node of Ranvier length may be adjusted to modify axonal conduction velocity and hence neural activity and function (Arancibia-Carcamo et al., 2017). Intravitreally administered AAV vectors that include BDNF maintain the paranodal gap at uninjured levels. BDNF interaction with TrkB mediates Fyn kinase activation and may result in the regulation of Na_v in the node of Ranvier (Ahn et al., 2007). While the administration of AAV2-CRMP2T555A-GFP alone is not sufficient in preserving the precise parameters of node paranode composition, specifically the paranodal gap (Ahn et al., 2007; Hilborn et al., 1998), it can preserve the proportion of typical node/paranode complexes including heminodes.

Here we confirm myelin thinning and increased G-ratio association with secondary degeneration in partial ON injury (Payne et al., 2012) and demonstrate for the first time these changes were reversed by AAV mediated treatment with BDNF and/or phospho-resistant CRMP2. However, axon size was not affected by the growth factor treatments. The thickness of the myelin sheath reflects a combination of the number of intraperiodic lines and tightness/looseness of lamellae (Payne et al., 2012), raising the question as to whether viral vector mediated increases in myelin thickness are due to preservation of existing myelin sheath or remyelination? Although we did not assess the parameters to address this, others have demonstrated BDNF/TrkB activation mediates MAPK/Erk signalling within oligodendrocytes and that this can function to maintain myelin function and increase myelin thickness (Ishii et al., 2013; Michel et al., 2015; Xiao et al., 2010). TrkB activation by elevating BDNF levels promotes remyelination in vivo following ischemic stroke (Ramos-Cejudo et al., 2015) spinal cord injury (McTigue et al., 1998) and cuprizone mediated

demyelination (Fulmer et al., 2014). Alternatively, the AAV BDNF and phospho-resistant CRMP2 viral vector mediated effect on myelination and G-ratio could be a consequence of the 'inside-out' model of neuroprotection, consequent of enhanced axonal integrity.

Myelin decompaction is also a persistent, key feature of secondary degeneration. Decompacted ON axons were observed in normal uninjured axons, and to a much greater extent, following ON injury. Decompaction in the absence of axonal lesion is likely associated with oligodendrocyte turnover in mature nerve, although myelin decompaction may also in part be an artefact of the fixation process of electron microscopy (Dawson et al., 2003; Marinkovic et al., 2009). Treatment with AAV mediated BDNF alone was protective in all degrees of decompaction, however the therapeutic efficacy of phospho-resistant CRMP2T555A was only effective at lower rates of decompaction. Intriguingly, similar to RGC somata numbers in ventral retina, CRMP2 attenuated the therapeutic capacity of BDNF in axonal decompaction exceeding 20%. Further, the relationship between myelin thickness and axon calibre is generally strongly positive (Giacci et al., 2018; Guy et al., 1989), but after phospho-resistant CRMP2 treatment there was no correlation between axon calibre and myelin thickness, with myelin thickness consistently limited to about 0.1µm. Axonal injury has been extensively associated with myelin pathology including demyelination, often followed by instances of remyelination or dysmyelination, consequent of abnormal myelination (Becker and McDonald, 2012; Blight, 1983). However, occurrences of remyelination of spared axons following axonal lesion have been littered with suboptimal myelin sheath, including abnormally thin myelin, shortened internodes and disruption to the normal linear relationship between axon diameter and myelin thickness (Nashmi and Fehlings, 2001; Scolding and Lassmann, 1996). Arguably chronic demyelination or suboptimal remyelination is a contributor to aberrant axonal signalling and dysfunction (Nashmi and Fehlings, 2001; Scolding and Lassmann, 1996). Abnormal myelination that is associated with injury, exacerbates the degenerative events due to added 'noise' and is arguably no more beneficial than the absence of myelination (Becker and McDonald, 2012), and this potentially deleterious process is inhibited by CRMP2 by limiting myelin thickness and disrupting the correlation between axon calibre and myelin thickness.

In conclusion, our results suggest some dissociation between the processes of axonal loss and cell death in response to partial ON injury. Consequently, successful therapeutic intervention

is dependent on an orchestrated and appropriately timed response to secondary degeneration events in both the cell body and axon. Vector-mediated delivery of BDNF and/or CRMP2T555A both showed neuroprotective effects in the retina, but intravitreal injection of AAV2-BDNF in particular was more effective in ventral retina solely vulnerable to secondary degenerative events, and this vector had a greater impact on preserving visual behaviour. Both vectors prevented axonal die-back in the ON, but BDNF better maintained aspects of myelin integrity, and co-delivery of AAV2-CRMP2T555A-GFP occasionally reduced the efficacy of BDNF in this injury model of secondary degeneration (Table 1). The complex interactions seen in the retina and ON in primary versus secondary degenerative events presumably reflects the different biological activities of BDNF and CRMP2, the former likely to influence primarily TrkB signalling in RGC soma (Almasieh et al., 2012; Chitranshi et al., 2019; Harvey et al., 2012; Osborne et al., 2018), the latter having a greater impact on stabilising distal axonal integrity, microtubule dynamics and anterograde transport of neuronal growth related vesicular cargo (Bretin et al., 2005; Numata-Uematsu et al., 2019; Wang et al., 2015; Yuasa-Kawada et al., 2003; Zhang and Koch, 2017) . This is of particular relevance during axonogenesis and elongation whereby the alternatively spliced isoform of CRMP2A can be stabilised in the distal axon by the prolyl isomerase Pin1 (Balastik et al., 2015). Whether AAV2-CRMP2T555A overexpression in PT axons was also able to stabilise CRMP2A in the ON to limit myelin decompaction requires further investigation. These differences in efficacy may additionally be influenced by the fact that degenerative events in the cell body and axon can be initiated by different mechanisms (Almasieh et al., 2012; Casas et al., 2015; Munemasa and Kitaoka, 2012; Wang et al., 2012; Yu et al., 2013).

From a broader perspective, the protective effects of AAV-BDNF are well-established in diverse CNS injury models and neurodegenerative conditions. Delivery of AAV2 encoding the mutant, phospho-resistant, version of CRMP2 has been shown to reduce axonopathy and demyelination in experimental models of multiple sclerosis (Lee et al., 2019; Petratos et al., 2012), but the present data suggest that this vector may also be an effective therapy for other neurodegenerative conditions known to be associated with CRMP2 phosphorylation, including brain and spinal cord trauma (Nagai et al., 2016; Sekine et al., 2019; Taghian et al., 2012; Zhang and Koch, 2017), glaucoma (Wang et al., 2015), and amyotrophic lateral sclerosis (Numata-Uematsu et al., 2019).

Acknowledgements

We thank Michael Archer for assistance with EM tissue preparation and imaging. The authors thank the facilities, scientific and technical assistance of the Australia Microscopy and Microanalysis Research Facility at the Centre for Microscopy and Microanalysis, The University of Western Australia. MF has been supported by an NHMRC Career Development Fellowship (APP1087114).

Figure 1: Optokinetic nystagmus test of visual function three months following partial ON transection and therapeutic administration of BDNF and phospho-mutant CRMP2. (A) Schematic illustrating positioning of test animal inside the optokinetic nystagmus apparatus in relation to camera. (B) Satellite view schematic illustrating animal response to rotating drum and three types of tracking movement categorized as smooth, partial and micro pursuit. (C) Optokinetic nystagmus was assessed with mean (+ SEM) of total numbers of smooth, partial and micro pursuits in animals that had undergone the partial ON transection and were treated with vehicle AAV2-GFP or therapeutic AAV2-BDNF, AAV2-CRMP2T555A-GFP or AAV2-BDNF plus AAV2-CRMP2T555A-GFP. (D) and (E) represent mean smooth pursuits and fast resets respectively. Significant differences between experimental groups are indicated by *$p<0.05$, one-way ANOVA.

Figure 2: RGC survival when treated with virally administered BDNF and/or phospho-mutant CRMP2 following partial transection (PT) injury of the ON. (A) Schematic of the retina depicting the sites of the RGC counts. Total numbers of RGCs were counted using the optical fractionator method in three fields of view of ~ 200 - 300µm linear length for each of dorsal, central and ventral retina. RGC were quantified on 20µm thick retinal sections immunostained for βIII-tubulin$^+$, Brn3A$^+$ and Hoechst. Arrow indicates RGC identified with: (B) βIII-tubulin surrounding a Hoechst labelled nucleus, (C) labelled with Brn3A$^+$ (D) and an overlay of Hoechst, βIII-tubulin$^+$ and Brn3A$^+$. (E) The proportion of βIII-tubulin$^+$ RGCs that are Brn3A$^+$, (* $p<0.05$, **$p<0.01$, ***$p<0.001$, ****$p<0.0001$ one-way ANOVA). Scale bar for all micrographs =100µm. (F) The mean number (+ SEM) of all surviving βIII-tubulin$^+$ and Brn3A$^+$ RGCs per mm^2 in normal uninjured retina, and retinas treated with AAV2-GFP, AAV2-BDNF, AAV2-CRMP2T555A-GFP or a combination of AAV2-BDNF and AAV2-CRMP2T555A-GFP, in dorsal, (G) central and (H) ventral retina following PT injury.

Figure 3: Axonal density and βIII-tubulin immunointensity following treatment with AAV2 administered BDNF and/or phospho-mutant CRMP2 after ON injury. (A) Number (+ SEM) of myelinated axons per mm^2 in ventral nerve semi-thin sections in normal uninjured ON, and nerves from retinas transduced with AAV2-GFP, AAV2-BDNF, AAV2-CRMP2T555A-GFP and a combination of AAV2-BDNF and AAV2-CRMP2T555A-GFP after PT injury (N = 3-4 per group). (B) Schematic diagram showing field of view sampled in ventral ON for axon counts. Scale bar = 100µm. (C) βIII-tubulin immunointensity in the

ventral ON assessed using area above set threshold for normal uninjured ON, and nerves treated with AAV2-GFP, AAV2-BDNF, AAV2-CRMP2T555A-GFP and a combination of AAV2-BDNF and AAV2-CRMP2T555A-GFP after ON injury. (D) Immunohistochemical assessment of area above threshold performed in ventral aspect of ON below injury site in longitudinal sections. Scale bar = 50 µm. Representative images of axonal density in ventral ON semi-thin sections in (E) normal uninjured animals (F) injured animals treated with AAV2-GFP and (G) injured animals treated with a combination of AAV2-BDNF and AAV2-CRMP2T555A-GFP. Scale bar = 1 µm. Representative images of ventral ON immunostained with βIII-tubulin in (H) normal uninjured animals (I) injured animals treated with AAV2-GFP and (J) injured animals treated with a combination of AAV2-BDNF and AAV2-CRMP2T555A-GFP. Scale bar = 50µm. (K) representative images of transverse sections of normal and injured ON (L) ON diameter (µm +SEM) and (M) ventral ON area (mm^2+SEM) (n=4, pooling of 6 images for each animal, *p<0.05, **p<0.01, ***p<0.001, ****p<0.0001 one-way ANOVA).

Figure 4: Node/paranode complex changes in ventral ON when treated with virally administered BDNF and/or phospho-mutant CRMP2 after ON injury. Nodal length (µm + SEM) of (A) total node/paranode complexes indicated by $Caspr^+$ paranodes. (B) Typical complexes selected only when $Caspr^+$ immunostained paranodes flank a βIII-tubulin immunostained node. Results are expressed as the mean of ~100 complexes per animal. Representative images of node/paranode (C) total complexes and (D) typical complexes in normal rats and AAV2-GFP treated injured animals. (E) Images of location of node and paranode length measures. (F) A representative orthogonal z-projection of βIII-tubulin and $Caspr^+$ immunopositive node and paranode structures respectively within the node of Ranvier from a normal ventral ON; scale bar = 5 µm. (G) Mean + SEM percentage of atypical node/ paranode complexes βIII-tubulin and Caspr immunostained uninjured ON, and nerves from eyes injected with AAV2-GFP, AAV2-BDNF, AAV2-CRMP2T555A-GFP and a combination of AAV2-BDNF and AAV2-CRMP2T555A-GFP after PT injury. Mean number + SEM of (H) typical complexes; βIII-tubulin immunostained node, flanked by two-Caspr immunostained paranodes, (I) heminode complexes; βIII-tubulin immunostained node, flanked by one-Caspr immunostained paranode and (J) single nodes; a Caspr immunostained paranode, in ventral ON. (K) Representative images of typical, heminode and single node complexes.

Figure 5: Quantification of axonal and myelin changes in RGC axons from retinas treated with virally administered BDNF and/or phospho-mutant CRMP2. Axonal (A) G-ratio, the ratio of the inner axonal diameter to the total outer diameter (mean + SEM) and (B) myelin thickness (mean + SEM) of normally myelinated axons. (C) Frequency histograms of axon diameter of all quantified normally myelinated axons in normal uninjured ON sections, and nerves from eyes treated with AAV2-GFP, AAV2-BDNF, AAV2-CRMP2T555A-GFP and a combination of AAV2-BDNF and AAV2-CRMP2T555A-GFP after PT injury (N = 3-4 per group). Data are expressed as frequency (%) and mean axon diameter ± SD. (D) Myelin decompaction assessed as percent (+ SEM) of total fibre circumference with myelin disruption/ decompaction. Three levels of myelin decompaction were used to categorise degree of damage, 0 to 15%, 20 to 30% and over 30%. Axons with myelin decompaction ≤15% were categorised as normally myelinated axons. Representative images of myelin decompaction quantification indicate (E) 10%, (F) 30% and (G) 90% myelin decompaction. (H) Myelin thickness is plotted using line of best fit as a function of axonal diameter of all normally myelinated axons. Significant differences between experimental groups are indicated by *p<0.05, **p<0.01, ***p<0.001, ****p<0.0001, one-way ANOVA.

Supplementary Figure 1: GFP expression in rat retina and ON three months following a rAAV2 intravitreal delivery of BDNF and phospho-mutant CRMP2. (A) Percentage of RGCs transduced with AAV2-BDNF, AAV2-CRMP2T555A-GFP and AAV2-BDNF plus AAV2-CRMP2T555A-GFP. (B) and (C) representative retinal sections immunolabeled for GFP, βIII-tubulin and Hoechst showing non-RGCs and β III positive RGCs transduced with GFP (arrows) respectively. (D) Representative retinal section of GFP transduced cell nuclei. (E) Comparison of area above threshold (+SEM) in axons immunolabeled with GFP following transduction with AAV2-BDNF, AAV2-CRMP2T555A-GFP and AAV2-BDNF + AAV2-CRMP2T555A-GFP. (F) and (G) AAV2-CRMP2T555A-GFP transduced ONs immunolabeled with GFP and βIII-tubulin respectively. (H) Co labelling of β III labelled axons with GFP. Scale bar = 50 µm.

Supplementary Figure 2: RGC transduction with viral vectors reduces oxidative stress but not inflammatory cell markers in injured ventral ON. (A) Immunointensity of oxidative stress marker HNE using mean (+ SEM) area above set threshold in normal uninjured animals and treated with vehicle AAV2-GFP or therapeutic AAV2-BDNF, AAV2-CRMP2T555A-GFP or AAV2-BDNF plus AAV2-CRMP2T555A-GFP after ON injury. Representative images of HNE (green) in (B) normal (C) AAV2-GFP treated and (D) AAV2-BDNF plus AAV2-CRMP2T555A-GFP sections of ventral ON. Scale bar = 50 µm. (E) The mean (+SEM) area above threshold of Iba1-positive microglia/ macrophages in normal animals and treated after ON injury. (F) Representative images of Iba1-positive microglia/ macrophages (magenta) in normal (G) Iba1-positive microglia/ macrophages (H) AAV2-BDNF plus AAV2-CRMP2T555A-GFP sections of ventral ON. Scale bar = 50 µm. Significant differences between experimental groups are indicated by *p<0.05, **p<0.01, one-way ANOVA.

Supplementary Figure 3: Combined RGC counts from central and ventral retina. The mean number (+ SEM) of all surviving βIII-tubulin^{+} RGCs per mm^{2} in normal uninjured retina, and retinas treated with AAV2-GFP, AAV2-BDNF, AAV2-CRMP2T555A-GFP or a combination of AAV2-BDNF and AAV2-CRMP2T555A-GFP central and ventral retina following PT injury. * p<0.05, **p<0.01, ***p<0.001, ****p<0.0001 one-way ANOVA.

References

Abdeljalil, J., Hamid, M., Abdel-Mouttalib, O., Stephane, R., Raymond, R., Johan, A., Jose, S., Pierre, C., Serge, P., 2005. The optomotor response: a robust first-line visual screening method for mice. Vision Res 45, 1439-1446.

Ahn, M., Beacham, D., Westenbroek, R.E., Scheuer, T., Catterall, W.A., 2007. Regulation of Na(v)1.2 channels by brain-derived neurotrophic factor, TrkB, and associated Fyn kinase. J Neurosci 27, 11533-11542.

Almasieh, M., Wilson, A.M., Morquette, B., Cueva Vargas, J.L., Di Polo, A., 2012. The molecular basis of retinal ganglion cell death in glaucoma. Prog Retin Eye Res 31, 152-181.

Arancibia-Carcamo, I.L., Ford, M.C., Cossell, L., Ishida, K., Tohyama, K., Attwell, D., 2017. Node of Ranvier length as a potential regulator of myelinated axon conduction speed. Elife 6.

Arimura, N., Hattori, A., Kimura, T., Nakamuta, S., Funahashi, Y., Hirotsune, S., Furuta, K., Urano, T., Toyoshima, Y.Y., Kaibuchi, K., 2009a. CRMP-2 directly binds to cytoplasmic dynein and interferes with its activity. J Neurochem 111, 380-390.

Arimura, N., Kimura, T., Nakamuta, S., Taya, S., Funahashi, Y., Hattori, A., Shimada, A., Menager, C., Kawabata, S., Fujii, K., Iwamatsu, A., Segal, R.A., Fukuda, M., Kaibuchi, K., 2009b. Anterograde transport of TrkB in axons is mediated by direct interaction with Slp1 and Rab27. Dev Cell 16, 675-686.

Arimura, N., Menager, C., Kawano, Y., Yoshimura, T., Kawabata, S., Hattori, A., Fukata, Y., Amano, M., Goshima, Y., Inagaki, M., Morone, N., Usukura, J., Kaibuchi, K., 2005. Phosphorylation by Rho kinase regulates CRMP-2 activity in growth cones. Mol Cell Biol 25, 9973-9984.

Balastik, M., Zhou, X.Z., Alberich-Jorda, M., Weissova, R., Ziak, J., Pazyra-Murphy, M.F., Cosker, K.E., Machonova, O., Kozmikova, I., Chen, C.H., Pastorino, L., Asara, J.M., Cole, A., Sutherland, C., Segal, R.A., Lu, K.P., 2015. Prolyl Isomerase Pin1 Regulates Axon Guidance by Stabilizing CRMP2A Selectively in Distal Axons. Cell Rep 13, 812-828.

Baumgartner, B.J., Shine, H.D., 1997. Targeted transduction of CNS neurons with adenoviral vectors carrying neurotrophic factor genes confers neuroprotection that exceeds the transduced population. J Neurosci 17, 6504-6511.

Becker, D., McDonald, J.W., 3rd, 2012. Approaches to repairing the damaged spinal cord: overview. Handb Clin Neurol 109, 445-461.

Berkelaar, M., Clarke, D.B., Wang, Y.C., Bray, G.M., Aguayo, A.J., 1994. Axotomy results in delayed death and apoptosis of retinal ganglion cells in adult rats. J Neurosci 14, 4368-4374.

Blight, A.R., 1983. Cellular morphology of chronic spinal cord injury in the cat: analysis of myelinated axons by line-sampling. Neuroscience 10, 521-543.

Bretin, S., Reibel, S., Charrier, E., Maus-Moatti, M., Auvergnon, N., Thevenoux, A., Glowinski, J., Rogemond, V., Premont, J., Honnorat, J., Gauchy, C., 2005. Differential expression of CRMP1, CRMP2A, CRMP2B, and CRMP5 in axons or dendrites of distinct neurons in the mouse brain. J Comp Neurol 486, 1-17.

Brittain, J.M., Wang, Y., Eruvwetere, O., Khanna, R., 2012. Cdk5-mediated phosphorylation of CRMP-2 enhances its interaction with CaV2.2. FEBS Lett 586, 3813-3818.

Casas, C., Isus, L., Herrando-Grabulosa, M., Mancuso, F.M., Borras, E., Sabido, E., Fores, J., Aloy, P., 2015. Network-based proteomic approaches reveal the neurodegenerative, neuroprotective and pain-related mechanisms involved after retrograde axonal damage. Sci Rep 5, 9185.

Chen, A., Xiong, L.J., Tong, Y., Mao, M., 2013. The neuroprotective roles of BDNF in hypoxic ischemic brain injury. Biomed Rep 1, 167-176.

Chew, L.A., Khanna, R., 2018. CRMP2 and voltage-gated ion channels: potential roles in neuropathic pain. Neuronal Signal 2.

Chiha, W., LeVaillant, C.J., Bartlett, C.A., Hewitt, A.W., Melton, P.E., Fitzgerald, M., Harvey, A.R., 2018. Retinal genes are differentially expressed in areas of primary versus secondary degeneration following partial optic nerve injury. PLoS One 13, e0192348.

Chitranshi, N., Dheer, Y., Mirzaei, M., Wu, Y., Salekdeh, G.H., Abbasi, M., Gupta, V., Vander Wall, R., You, Y., Graham, S.L., Gupta, V., 2019. Loss of Shp2 Rescues BDNF/TrkB Signaling and Contributes to Improved Retinal Ganglion Cell Neuroprotection. Mol Ther 27, 424-441.

Chomiak, T., Hu, B., 2009. What is the optimal value of the g-ratio for myelinated fibers in the rat CNS? A theoretical approach. PLoS One 4, e7754.

Dawson, M.R., Polito, A., Levine, J.M., Reynolds, R., 2003. NG2-expressing glial progenitor cells: an abundant and widespread population of cycling cells in the adult rat CNS. Mol Cell Neurosci 24, 476-488.

de Winter, F., Cui, Q., Symons, N., Verhaagen, J., Harvey, A.R., 2004. Expression of class-3 semaphorins and their receptors in the neonatal and adult rat retina. Invest Ophthalmol Vis Sci 45, 4554-4562.

Di Polo, A., Aigner, L.J., Dunn, R.J., Bray, G.M., Aguayo, A.J., 1998. Prolonged delivery of brain-derived neurotrophic factor by adenovirus-infected Muller cells temporarily rescues injured retinal ganglion cells. Proc Natl Acad Sci U S A 95, 3978-3983.

Dubey, J., Ratnakaran, N., Koushika, S.P., 2015. Neurodegeneration and microtubule dynamics: death by a thousand cuts. Front Cell Neurosci 9, 343.

Eichler, M.E., Rich, K.M., 1989. Death of sensory ganglion neurons after acute withdrawal of nerve growth factor in dissociated cell cultures. Brain Res 482, 340-346.

Evans, K.J., Gomes, E.R., Reisenweber, S.M., Gundersen, G.G., Lauring, B.P., 2005. Linking axonal degeneration to microtubule remodeling by Spastin-mediated microtubule severing. J Cell Biol 168, 599-606.

Fisher, K.J., Gao, G.P., Weitzman, M.D., DeMatteo, R., Burda, J.F., Wilson, J.M., 1996. Transduction with recombinant adeno-associated virus for gene therapy is limited by leading-strand synthesis. J Virol 70, 520-532.

Fitzgerald, M., Bartlett, C.A., Harvey, A.R., Dunlop, S.A., 2010. Early events of secondary degeneration after partial optic nerve transection: an immunohistochemical study. J Neurotrauma 27, 439-452.

Fitzgerald, M., Payne, S.C., Bartlett, C.A., Evill, L., Harvey, A.R., Dunlop, S.A., 2009. Secondary retinal ganglion cell death and the neuroprotective effects of the calcium channel blocker lomerizine. Invest Ophthalmol Vis Sci 50, 5456-5462.

Frim, D.M., Uhler, T.A., Galpern, W.R., Beal, M.F., Breakefield, X.O., Isacson, O., 1994. Implanted fibroblasts genetically engineered to produce brain-derived neurotrophic factor prevent 1-methyl-4-phenylpyridinium toxicity to dopaminergic neurons in the rat. Proc Natl Acad Sci U S A 91, 5104-5108.

Fu, Y., Sun, W., Shi, Y., Shi, R., Cheng, J.X., 2009. Glutamate excitotoxicity inflicts paranodal myelin splitting and retraction. PLoS One 4, e6705.

Fukata, Y., Itoh, T.J., Kimura, T., Menager, C., Nishimura, T., Shiromizu, T., Watanabe, H., Inagaki, N., Iwamatsu, A., Hotani, H., Kaibuchi, K., 2002. CRMP-2 binds to tubulin heterodimers to promote microtubule assembly. Nat Cell Biol 4, 583-591.

Fulmer, C.G., VonDran, M.W., Stillman, A.A., Huang, Y., Hempstead, B.L., Dreyfus, C.F., 2014. Astrocyte-derived BDNF supports myelin protein synthesis after cuprizone-induced demyelination. J Neurosci 34, 8186-8196.

Geden, M.J., Deshmukh, M., 2016. Axon degeneration: context defines distinct pathways. Curr Opin Neurobiol 39, 108-115.

Giacci, M.K., Bartlett, C.A., Huynh, M., Kilburn, M.R., Dunlop, S.A., Fitzgerald, M., 2018. Three dimensional electron microscopy reveals changing axonal and myelin morphology along normal and partially injured optic nerves. Sci Rep 8, 3979.

Gundersen, H.J., 1986. Stereology of arbitrary particles. A review of unbiased number and size estimators and the presentation of some new ones, in memory of William R. Thompson. J Microsc 143, 3-45.

Gutierrez, R., Boison, D., Heinemann, U., Stoffel, W., 1995. Decompaction of CNS myelin leads to a reduction of the conduction velocity of action potentials in optic nerve. Neuroscience Letters 195, 93-96.

Guy, J., Ellis, E.A., Kelley, K., Hope, G.M., 1989. Spectra of G ratio, myelin sheath thickness, and axon and fiber diameter in the guinea pig optic nerve. J Comp Neurol 287, 446-454.

Harvey, A.R., Hu, Y., Leaver, S.G., Mellough, C.B., Park, K., Verhaagen, J., Plant, G.W., Cui, Q., 2006. Gene therapy and transplantation in CNS repair: the visual system. Prog Retin Eye Res 25, 449-489.

Harvey, A.R., Kamphuis, W., Eggers, R., Symons, N.A., Blits, B., Niclou, S., Boer, G.J., Verhaagen, J., 2002. Intravitreal injection of adeno-associated viral vectors results in the transduction of different types of retinal neurons in neonatal and adult rats: a comparison with lentiviral vectors. Mol Cell Neurosci 21, 141-157.

Harvey, A.R., Lovett, S.J., Majda, B.T., Yoon, J.H., Wheeler, L.P., Hodgetts, S.I., 2015. Neurotrophic factors for spinal cord repair: Which, where, how and when to apply, and for what period of time? Brain Res 1619, 36-71.

Harvey, A.R., Ooi, J.W., Rodger, J., 2012. Neurotrophic factors and the regeneration of adult retinal ganglion cell axons. Int Rev Neurobiol 106, 1-33.

Hellstrom, M., Pollett, M.A., Harvey, A.R., 2011. Post-injury delivery of rAAV2-CNTF combined with short-term pharmacotherapy is neuroprotective and promotes extensive axonal regeneration after optic nerve trauma. J Neurotrauma 28, 2475-2483.

Henry, R.A., Hughes, S.M., Connor, B., 2007. AAV-mediated delivery of BDNF augments neurogenesis in the normal and quinolinic acid-lesioned adult rat brain. Eur J Neurosci 25, 3513-3525.

Hilborn, M.D., Vaillancourt, R.R., Rane, S.G., 1998. Growth factor receptor tyrosine kinases acutely regulate neuronal sodium channels through the src signaling pathway. J Neurosci 18, 590-600.

Huang, E.J., Reichardt, L.F., 2001. Neurotrophins: roles in neuronal development and function. Annu Rev Neurosci 24, 677-736.

Igarashi, T., Miyake, K., Kobayashi, M., Kameya, S., Fujimoto, C., Nakamoto, K., Takahashi, H., Igarashi, T., Miyake, N., Iijima, O., Hirai, Y., Shimada, T., Okada, T., Takahashi, H., 2016. Tyrosine triple mutated AAV2-BDNF gene therapy in a rat model of transient IOP elevation. Mol Vis 22, 816-826.

Inagaki, N., Chihara, K., Arimura, N., Menager, C., Kawano, Y., Matsuo, N., Nishimura, T., Amano, M., Kaibuchi, K., 2001. CRMP-2 induces axons in cultured hippocampal neurons. Nat Neurosci 4, 781-782.

Isenmann, S., Schmeer, C., Kretz, A., 2004. How to keep injured CNS neurons viable--strategies for neuroprotection and gene transfer to retinal ganglion cells. Mol Cell Neurosci 26, 1-16.

Isenmann, S., Wahl, C., Krajewski, S., Reed, J.C., Bahr, M., 1997. Up-regulation of Bax protein in degenerating retinal ganglion cells precedes apoptotic cell death after optic nerve lesion in the rat. Eur J Neurosci 9, 1763-1772.

Ishii, A., Furusho, M., Bansal, R., 2013. Sustained activation of ERK1/2 MAPK in oligodendrocytes and schwann cells enhances myelin growth and stimulates oligodendrocyte progenitor expansion. J Neurosci 33, 175-186.

Jiao, S.S., Shen, L.L., Zhu, C., Bu, X.L., Liu, Y.H., Liu, C.H., Yao, X.Q., Zhang, L.L., Zhou, H.D., Walker, D.G., Tan, J., Gotz, J., Zhou, X.F., Wang, Y.J., 2016. Brain-derived neurotrophic factor protects against tau-related neurodegeneration of Alzheimer's disease. Transl Psychiatry 6, e907.

Kelly, M.J., O'Keeffe, G.W., Sullivan, A.M., 2015. Viral vector delivery of neurotrophic factors for Parkinson's disease therapy. Expert Rev Mol Med 17, e8.

Kimura, T., Watanabe, H., Iwamatsu, A., Kaibuchi, K., 2005. Tubulin and CRMP-2 complex is transported via Kinesin-1. J Neurochem 93, 1371-1382.

Kinoshita, Y., Kondo, S., Takahashi, K., Nagai, J., Wakatsuki, S., Araki, T., Goshima, Y., Ohshima, T., 2019. Genetic inhibition of CRMP2 phosphorylation delays Wallerian degeneration after optic nerve injury. Biochem Biophys Res Commun 514, 1037-1039.

Koeberle, P.D., Ball, A.K., 2002. Neurturin enhances the survival of axotomized retinal ganglion cells in vivo: combined effects with glial cell line-derived neurotrophic factor and brain-derived neurotrophic factor. Neuroscience 110, 555-567.

Kondo, S., Takahashi, K., Kinoshita, Y., Nagai, J., Wakatsuki, S., Araki, T., Goshima, Y., Ohshima, T., 2019. Genetic inhibition of CRMP2 phosphorylation at serine 522 promotes axonal regeneration after optic nerve injury. Sci Rep 9, 7188.

Kwon, B.K., Liu, J., Lam, C., Plunet, W., Oschipok, L.W., Hauswirth, W., Di Polo, A., Blesch, A., Tetzlaff, W., 2007. Brain-derived neurotrophic factor gene transfer with adeno-associated viral and lentiviral vectors prevents rubrospinal neuronal atrophy and stimulates regeneration-associated gene expression after acute cervical spinal cord injury. Spine (Phila Pa 1976) 32, 1164-1173.

Leaver, S.G., Cui, Q., Plant, G.W., Arulpragasam, A., Hisheh, S., Verhaagen, J., Harvey, A.R., 2006. AAV-mediated expression of CNTF promotes long-term survival and regeneration of adult rat retinal ganglion cells. Gene Ther 13, 1328-1341.

Lee, J.Y., Kim, M.J., Thomas, S., Oorschot, V., Ramm, G., Aui, P.M., Sekine, Y., Deliyanti, D., Wilkinson-Berka, J., Niego, B., Harvey, A.R., Theotokis, P., McLean, C., Strittmatter, S.M., Petratos, S., 2019. Limiting Neuronal Nogo Receptor 1 Signaling during Experimental Autoimmune Encephalomyelitis Preserves Axonal Transport and Abrogates Inflammatory Demyelination. J Neurosci 39, 5562-5580.

Leibinger, M., Andreadaki, A., Golla, R., Levin, E., Hilla, A.M., Diekmann, H., Fischer, D., 2017. Boosting CNS axon regeneration by harnessing antagonistic effects of GSK3 activity. Proc Natl Acad Sci U S A 114, E5454-E5463.

LeVaillant, C.J., Sharma, A., Muhling, J., Wheeler, L.P., Cozens, G.S., Hellstrom, M., Rodger, J., Harvey, A.R., 2016. Significant changes in endogenous retinal gene expression assessed 1 year after a single intraocular injection of AAV-CNTF or AAV-BDNF. Mol Ther Methods Clin Dev 3, 16078.

Levkovitch-Verbin, H., Dardik, R., Vander, S., Melamed, S., 2010. Mechanism of retinal ganglion cells death in secondary degeneration of the optic nerve. Exp Eye Res 91, 127-134.

Liz, M.A., Mar, F.M., Santos, T.E., Pimentel, H.I., Marques, A.M., Morgado, M.M., Vieira, S., Sousa, V.F., Pemble, H., Wittmann, T., Sutherland, C., Woodgett, J.R., Sousa, M.M., 2014. Neuronal deletion of GSK3beta increases microtubule speed in the growth cone and enhances axon regeneration via CRMP-2 and independently of MAP1B and CLASP2. BMC Biol 12, 47.

Luo, X., Salgueiro, Y., Beckerman, S.R., Lemmon, V.P., Tsoulfas, P., Park, K.K., 2013. Three-dimensional evaluation of retinal ganglion cell axon regeneration and pathfinding in whole mouse tissue after injury. Exp Neurol 247, 653-662.

Mansour-Robaey, S., Clarke, D.B., Wang, Y.C., Bray, G.M., Aguayo, A.J., 1994. Effects of ocular injury and administration of brain-derived neurotrophic factor on survival and regrowth of axotomized retinal ganglion cells. Proc Natl Acad Sci U S A 91, 1632-1636.

Marinkovic, S., Gibo, H., Todorovic, V., Antic, B., Kovacevic, D., Milisavljevic, M., Cetkovic, M., 2009. Ultrastructure and immunohistochemistry of the trigeminal peripheral myelinated axons in patients with neuralgia. Clin Neurol Neurosurg 111, 795-800.

Martin, K.R., Quigley, H.A., Zack, D.J., Levkovitch-Verbin, H., Kielczewski, J., Valenta, D., Baumrind, L., Pease, M.E., Klein, R.L., Hauswirth, W.W., 2003. Gene therapy with brain-derived neurotrophic factor as a protection: retinal ganglion cells in a rat glaucoma model. Invest Ophthalmol Vis Sci 44, 4357-4365.

McTigue, D.M., Horner, P.J., Stokes, B.T., Gage, F.H., 1998. Neurotrophin-3 and brain-derived neurotrophic factor induce oligodendrocyte proliferation and myelination of regenerating axons in the contused adult rat spinal cord. J Neurosci 18, 5354-5365.

Mead, B., Thompson, A., Scheven, B.A., Logan, A., Berry, M., Leadbeater, W., 2014. Comparative evaluation of methods for estimating retinal ganglion cell loss in retinal sections and wholemounts. PLoS One 9, e110612.

Mey, J., Thanos, S., 1993. Intravitreal injections of neurotrophic factors support the survival of axotomized retinal ganglion cells in adult rats in vivo. Brain Res 602, 304-317.

Michel, K., Zhao, T., Karl, M., Lewis, K., Fyffe-Maricich, S.L., 2015. Translational control of myelin basic protein expression by ERK2 MAP kinase regulates timely remyelination in the adult brain. J Neurosci 35, 7850-7865.

Miyata, S., Taniguchi, M., Koyama, Y., Shimizu, S., Tanaka, T., Yasuno, F., Yamamoto, A., Iida, H., Kudo, T., Katayama, T., Tohyama, M., 2016. Association between chronic stress-induced structural abnormalities in Ranvier nodes and reduced oligodendrocyte activity in major depression. Sci Rep 6, 23084.

Mizuguchi, H., Xu, Z., Ishii-Watabe, A., Uchida, E., Hayakawa, T., 2000. IRES-dependent second gene expression is significantly lower than cap-dependent first gene expression in a bicistronic vector. Mol Ther 1, 376-382.

Moore, J.W., Joyner, R.W., Brill, M.H., Waxman, S.D., Najar-Joa, M., 1978. Simulations of conduction in uniform myelinated fibers. Relative sensitivity to changes in nodal and internodal parameters. Biophys J 21, 147-160.

Munemasa, Y., Kitaoka, Y., 2012. Molecular mechanisms of retinal ganglion cell degeneration in glaucoma and future prospects for cell body and axonal protection. Front Cell Neurosci 6, 60.

Nadal-Nicolas, F.M., Jimenez-Lopez, M., Salinas-Navarro, M., Sobrado-Calvo, P., Alburquerque-Bejar, J.J., Vidal-Sanz, M., Agudo-Barriuso, M., 2012. Whole number, distribution and co-expression of brn3 transcription factors in retinal ganglion cells of adult albino and pigmented rats. PLoS One 7, e49830.

Nadal-Nicolas, F.M., Jimenez-Lopez, M., Sobrado-Calvo, P., Nieto-Lopez, L., Canovas-Martinez, I., Salinas-Navarro, M., Vidal-Sanz, M., Agudo, M., 2009. Brn3a as a marker of retinal ganglion cells: qualitative and quantitative time course studies in naive and optic nerve-injured retinas. Invest Ophthalmol Vis Sci 50, 3860-3868.

Nafissi, N., Foldvari, M., 2016. Neuroprotective therapies in glaucoma: I. Neurotrophic factor delivery. Wiley Interdiscip Rev Nanomed Nanobiotechnol 8, 240-254.

Nagai, J., Owada, K., Kitamura, Y., Goshima, Y., Ohshima, T., 2016. Inhibition of CRMP2 phosphorylation repairs CNS by regulating neurotrophic and inhibitory responses. Exp Neurol 277, 283-295.

Namekata, K., Harada, C., Guo, X., Kimura, A., Kittaka, D., Watanabe, H., Harada, T., 2012. Dock3 stimulates axonal outgrowth via GSK-3beta-mediated microtubule assembly. J Neurosci 32, 264-274.

Nashmi, R., Fehlings, M.G., 2001. Changes in axonal physiology and morphology after chronic compressive injury of the rat thoracic spinal cord. Neuroscience 104, 235-251.

Numata-Uematsu, Y., Wakatsuki, S., Nagano, S., Shibata, M., Sakai, K., Ichinohe, N., Mikoshiba, K., Ohshima, T., Yamashita, N., Goshima, Y., Araki, T., 2019. Inhibition of collapsin response mediator protein-2 phosphorylation ameliorates motor phenotype of ALS model mice expressing SOD1G93A. Neurosci Res 139, 63-68.

O'Hare Doig, R.L., Chiha, W., Giacci, M.K., Yates, N.J., Bartlett, C.A., Smith, N.M., Hodgetts, S.I., Harvey, A.R., Fitzgerald, M., 2017. Specific ion channels contribute to key elements of pathology during secondary degeneration following neurotrauma. BMC Neurosci 18, 62.

Osborne, A., Khatib, T.Z., Songra, L., Barber, A.C., Hall, K., Kong, G.Y.X., Widdowson, P.S., Martin, K.R., 2018. Neuroprotection of retinal ganglion cells by a novel gene therapy construct that achieves sustained enhancement of brain-derived neurotrophic factor/tropomyosin-related kinase receptor-B signaling. Cell Death Dis 9, 1007.

Payne, S.C., Bartlett, C.A., Harvey, A.R., Dunlop, S.A., Fitzgerald, M., 2012. Myelin sheath decompaction, axon swelling, and functional loss during chronic secondary degeneration in rat optic nerve. Invest Ophthalmol Vis Sci 53, 6093-6101.

Petratos, S., Ozturk, E., Azari, M.F., Kenny, R., Lee, J.Y., Magee, K.A., Harvey, A.R., McDonald, C., Taghian, K., Moussa, L., Mun Aui, P., Siatskas, C., Litwak, S., Fehlings, M.G., Strittmatter, S.M., Bernard, C.C., 2012. Limiting multiple sclerosis related axonopathy by blocking Nogo receptor and CRMP-2 phosphorylation. Brain 135, 1794-1818.

Poduslo, J.F., Curran, G.L., 1996. Permeability at the blood-brain and blood-nerve barriers of the neurotrophic factors: NGF, CNTF, NT-3, BDNF. Mol Brain Res 36, 280-286.

Popko, B., 2000. Myelin galactolipids: mediators of axon-glial interactions? Glia 29, 149-153.

Quigley, H.A., McKinnon, S.J., Zack, D.J., Pease, M.E., Kerrigan-Baumrind, L.A., Kerrigan, D.F., Mitchell, R.S., 2000. Retrograde axonal transport of BDNF in retinal ganglion cells is blocked by acute IOP elevation in rats. Invest Ophthalmol Vis Sci 41, 3460-3466.

Ramos-Cejudo, J., Gutierrez-Fernandez, M., Otero-Ortega, L., Rodriguez-Frutos, B., Fuentes, B., Vallejo-Cremades, M.T., Hernanz, T.N., Cerdan, S., Diez-Tejedor, E., 2015. Brain-derived neurotrophic factor administration mediated oligodendrocyte differentiation and myelin formation in subcortical ischemic stroke. Stroke 46, 221-228.

Rich, K.M., 1992. Neuronal death after trophic factor deprivation. J Neurotrauma 9 Suppl 1, S61-69.

Sarra, G.M., Stephens, C., Schlichtenbrede, F.C., Bainbridge, J.W., Thrasher, A.J., Luthert, P.J., Ali, R.R., 2002. Kinetics of transgene expression in mouse retina following sub-retinal injection of recombinant adeno-associated virus. Vision Res 42, 541-549.

Savigni, D.L., O'Hare Doig, R.L., Szymanski, C.R., Bartlett, C.A., Lozic, I., Smith, N.M., Fitzgerald, M., 2013. Three Ca2+ channel inhibitors in combination limit chronic secondary degeneration following neurotrauma. Neuropharmacology 75, 380-390.

Scolding, N., Lassmann, H., 1996. Demyelination and remyelination. Trends Neurosci 19, 1-2.

Sekine, Y., Algarate, P.T., Cafferty, W.B.J., Strittmatter, S.M., 2019. Plexina2 and CRMP2 Signaling Complex Is Activated by Nogo-A-Liganded Ngr1 to Restrict Corticospinal Axon Sprouting after Trauma. J Neurosci 39, 3204-3216.

Selt, M., Bartlett, C.A., Harvey, A.R., Dunlop, S.A., Fitzgerald, M., 2010. Limited restoration of visual function after partial optic nerve injury; a time course study using the calcium channel blocker lomerizine. Brain Res Bull 81, 467-471.

Sharma, A., Pollett, M.A., Plant, G.W., Harvey, A.R., 2012. Changes in mRNA expression of class 3 semaphorins and their receptors in the adult rat retino-collicular system after unilateral optic nerve injury. Invest Ophthalmol Vis Sci 53, 8367-8377.

Szymanski, C.R., Chiha, W., Morellini, N., Cummins, N., Bartlett, C.A., O'Hare Doig, R.L., Savigni, D.L., Payne, S.C., Harvey, A.R., Dunlop, S.A., Fitzgerald, M., 2013. Paranode Abnormalities and Oxidative Stress in Optic Nerve Vulnerable to Secondary Degeneration: Modulation by 670 nm Light Treatment. PLoS One 8, e66448.

Taghian, K., Lee, J.Y., Petratos, S., 2012. Phosphorylation and cleavage of the family of collapsin response mediator proteins may play a central role in neurodegeneration after CNS trauma. J Neurotrauma 29, 1728-1735.

Tejeda, G.S., Diaz-Guerra, M., 2017. Integral Characterization of Defective BDNF/TrkB Signalling in Neurological and Psychiatric Disorders Leads the Way to New Therapies. Int J Mol Sci 18.

Thomas, C.E., Birkett, D., Anozie, I., Castro, M.G., Lowenstein, P.R., 2001. Acute direct adenoviral vector cytotoxicity and chronic, but not acute, inflammatory responses correlate with decreased vector-mediated transgene expression in the brain. Mol Ther 3, 36-46.

Wang, Q., Vlkolinsky, R., Xie, M., Obenaus, A., Song, S.K., 2012. Diffusion tensor imaging detected optic nerve injury correlates with decreased compound action potentials after murine retinal ischemia. Invest Ophthalmol Vis Sci 53, 136-142.

Wang, X., Lin, J., Arzeno, A., Choi, J.Y., Boccio, J., Frieden, E., Bhargava, A., Maynard, G., Tsai, J.C., Strittmatter, S.M., 2015. Intravitreal delivery of human NgR-Fc decoy protein regenerates axons after optic nerve crush and protects ganglion cells in glaucoma models. Invest Ophthalmol Vis Sci 56, 1357-1366.

Waxman, S.G., 1980. Determinants of conduction velocity in myelinated nerve fibers. Muscle Nerve 3, 141-150.

Wilson, S.M., Xiong, W., Wang, Y., Ping, X., Head, J.D., Brittain, J.M., Gagare, P.D., Ramachandran, P.V., Jin, X., Khanna, R., 2012. Prevention of posttraumatic axon sprouting by blocking collapsin response mediator protein 2-mediated neurite outgrowth and tubulin polymerization. Neuroscience 210, 451-466.

Xiao, J., Wong, A.W., Willingham, M.M., van den Buuse, M., Kilpatrick, T.J., Murray, S.S., 2010. Brain-derived neurotrophic factor promotes central nervous system myelination via a direct effect upon oligodendrocytes. Neurosignals 18, 186-202.

Yamashita, N., Goshima, Y., 2012. Collapsin response mediator proteins regulate neuronal development and plasticity by switching their phosphorylation status. Mol Neurobiol 45, 234-246.

Yoshimura, T., Arimura, N., Kawano, Y., Kawabata, S., Wang, S., Kaibuchi, K., 2006. Ras regulates neuronal polarity via the PI3-kinase/Akt/GSK-3beta/CRMP-2 pathway. Biochem Biophys Res Commun 340, 62-68.

Yu, D.Y., Cringle, S.J., Balaratnasingam, C., Morgan, W.H., Yu, P.K., Su, E.N., 2013. Retinal ganglion cells: Energetics, compartmentation, axonal transport, cytoskeletons and vulnerability. Prog Retin Eye Res 36, 217-246.

Yuasa-Kawada, J., Suzuki, R., Kano, F., Ohkawara, T., Murata, M., Noda, M., 2003. Axonal morphogenesis controlled by antagonistic roles of two CRMP subtypes in microtubule organization. Eur J Neurosci 17, 2329-2343.

Zhang, J.N., Koch, J.C., 2017. Collapsin response mediator protein-2 plays a major protective role in acute axonal degeneration. Neural Regen Res 12, 692-695.

Zhang, Z., Ottens, A.K., Sadasivan, S., Kobeissy, F.H., Fang, T., Hayes, R.L., Wang, K.K., 2007. Calpain-mediated collapsin response mediator protein-1, -2, and -4 proteolysis after neurotoxic and traumatic brain injury. J Neurotrauma 24, 460-472.

Table 1

Table 1: Summary of outcomes 3 months following PT injury and treatment with AAV2-GFP, AAV2-BDNF, AAV2-CRMP2T555A, and combined AAV2-BDNF plus AAV2-CRMP2T555A.

Outcomes relative to uninjured control		Outcomes relative to injured AAV-GFP		
AAV2-GFP		AAV 2-BDNF	AAV2-CRMP2T555A-GFP	AAV2-BDNF/AAV2-CRMP2T555A-GFP
(-)	**Visual function**	↑	-	↑
↓	**RGC numbers**	↑	↑	↑
↓	**Axonal density**	↑	↑	↑
↓	**BIII tubulin III**	↑	↑	↑
↑	**Paranodal gap (all complexes)**	-	-	↓
↓	**Paranodal gap (β-III tubulin$^+$ complexes)**	↑	-	↑
↑	**% atypical nodes**	↓	↓	↓
↓	**% typical complex**	↑	↑	↑
↑	**% heminodes**	↓	↓	↓
↑	**% Single nodes**	-	-	-
↑	**G-ratio**	↓	↓	↓
↓	**Myelin thickness**	↑	↑	↑
↓	**% axons with 0-15% decompaction**	↑	↑	↑
↑	**% axons with 20-30% decompaction**	↓	-	-
↑	**% axons with >30% decompaction**	↓	-	-
↑	**Oxidative stress-HNE**	-	-	↓
↑	**Inflammatory cells-Iba1**	-	-	-

Outcome measures relate to secondary degeneration events in central and ventral retina (combined data), and in ventral ON. Symbols for AAV2-GFP treated animals indicate direction of change from normal uninjured animals. Following treatment with viral vectors, significant decreases relative to injured AAV2-GFP treated animals are shown as ↓, significant increases as ↑, no significant differences are indicated by - . (-), intermediate decrease but not significantly different from normal uninjured group.

Figure 1

Click here to download high resolution image

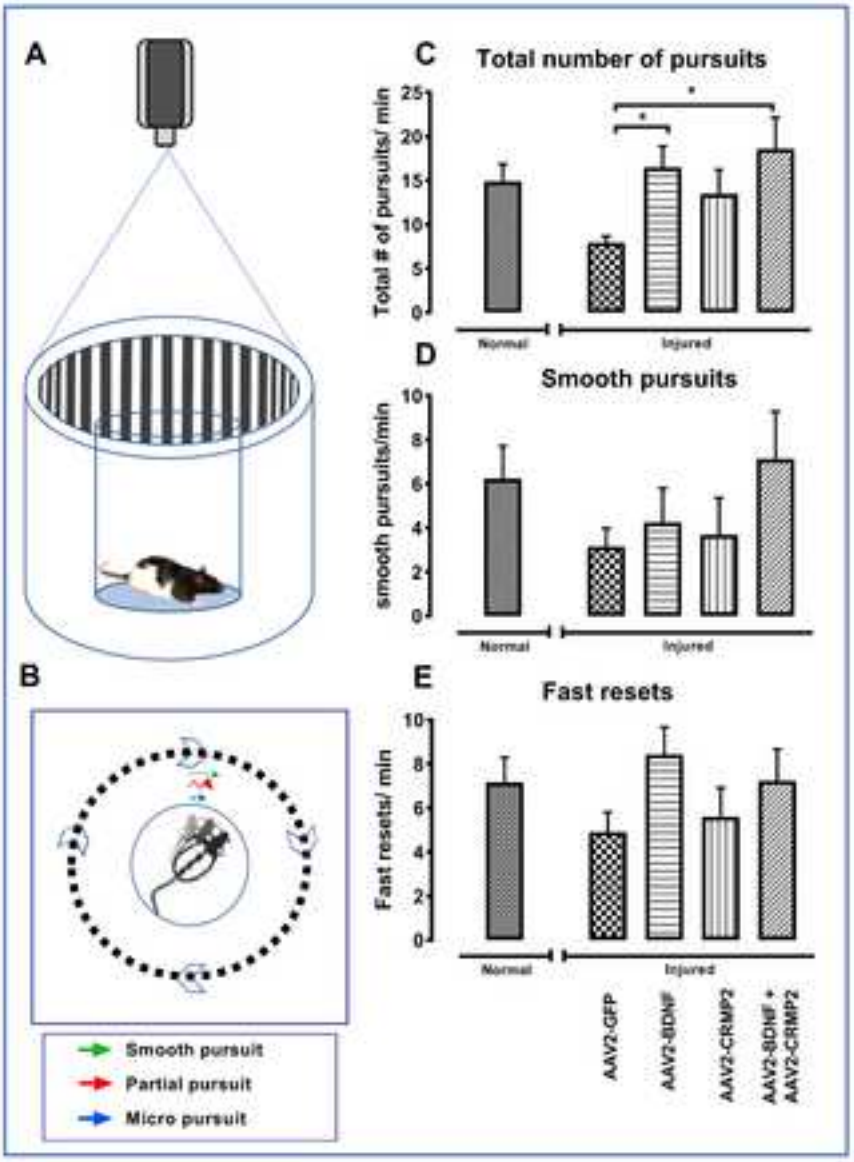

Figure 2

Click here to download high resolution image

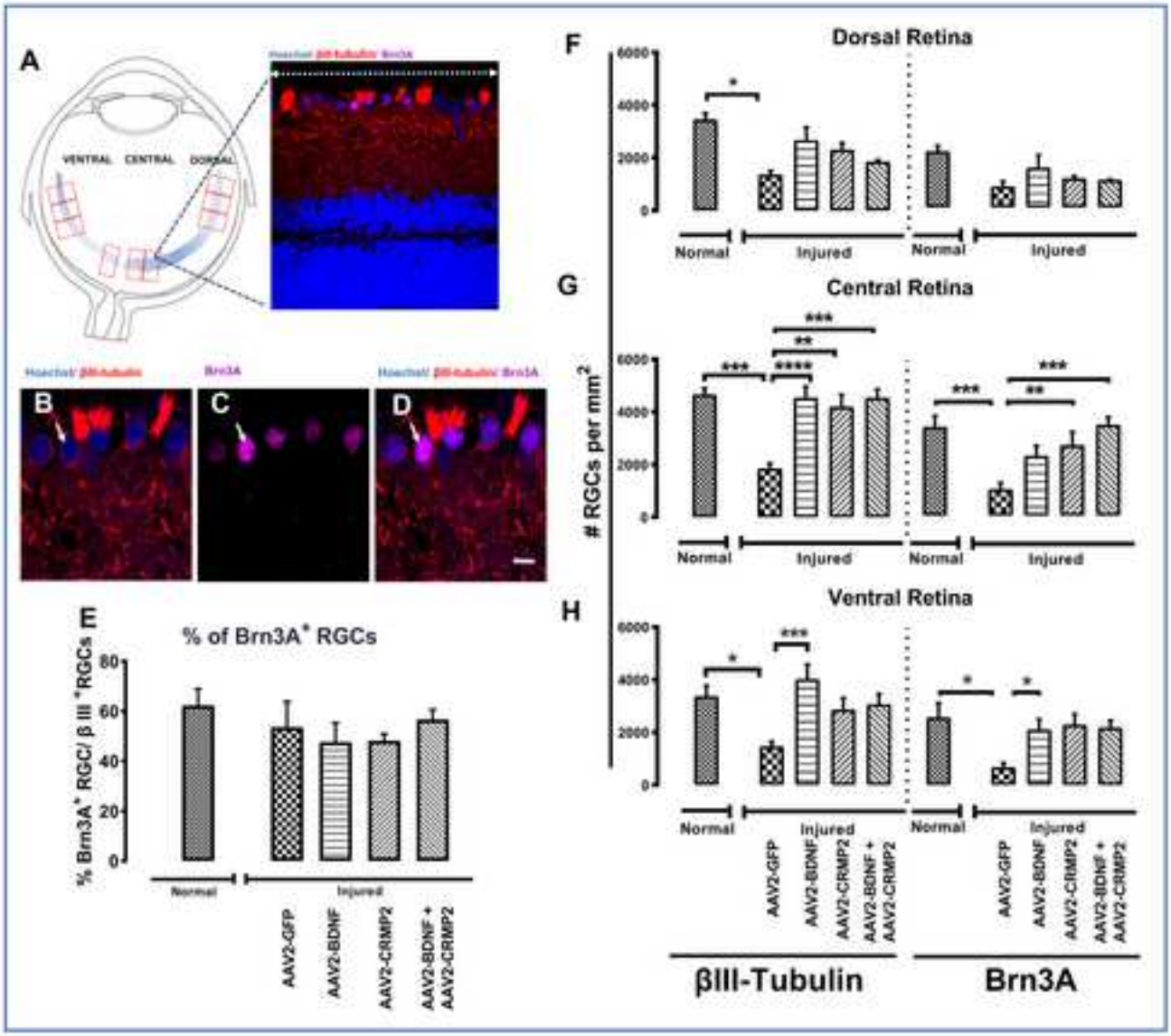

Figure 3

Click here to download high resolution image

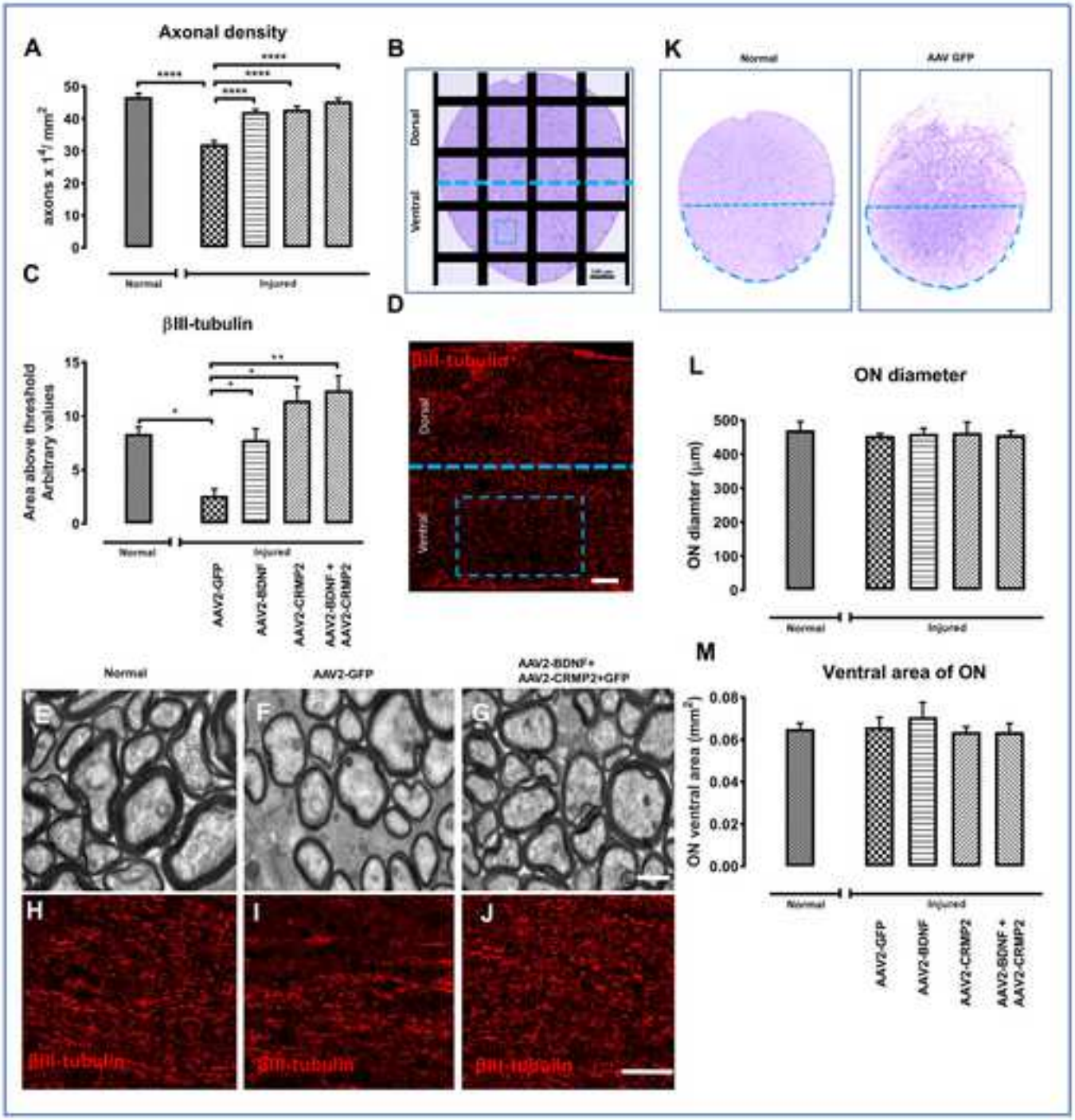

Figure 4

Click here to download high resolution image

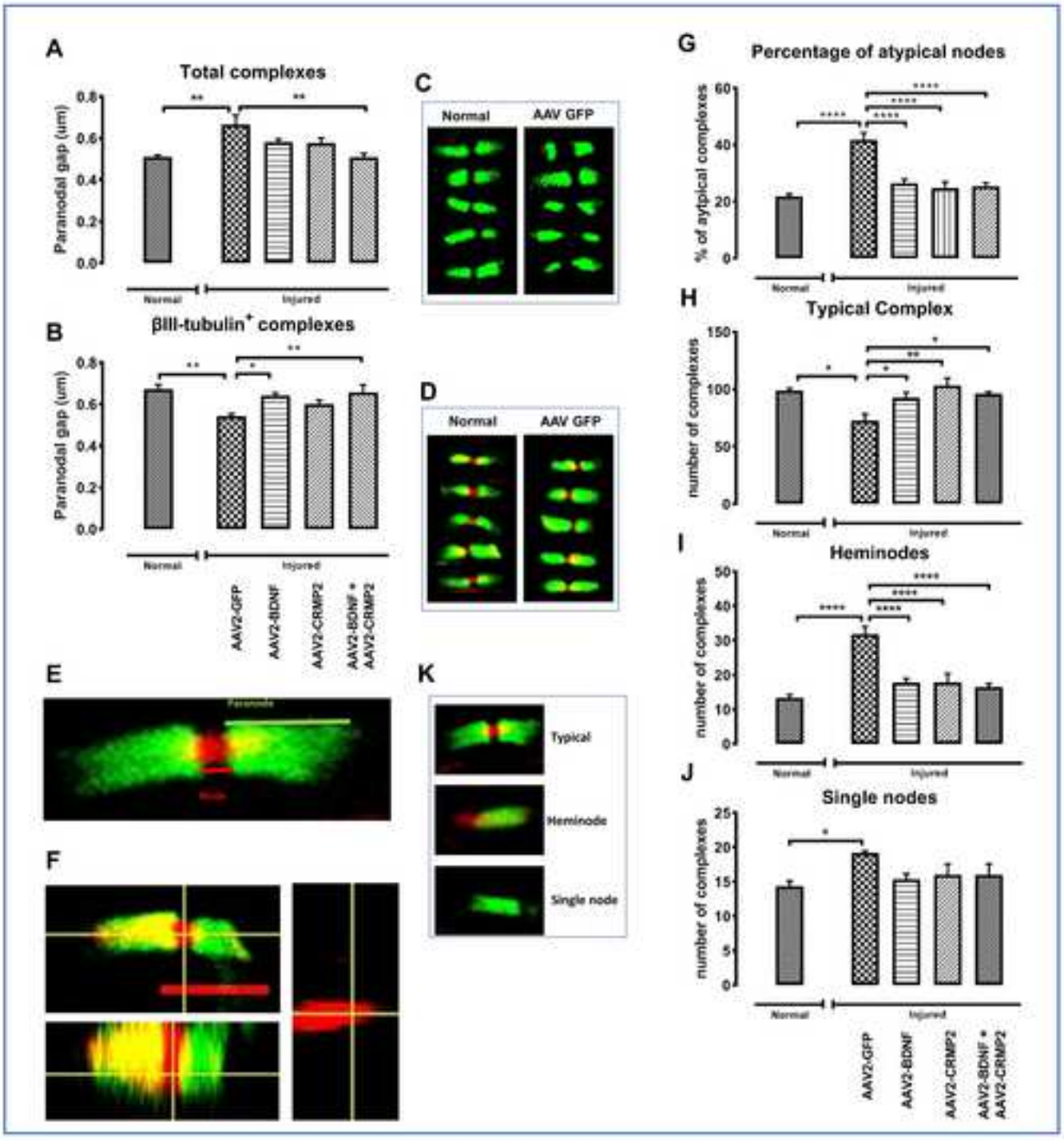

Figure 5

Click here to download high resolution image